ACCUMULATION AND MELT LAYERS, GREENLAND CLIMATE NETWORK (GC-NET)

Konrad Steffen, Thomas Philips, William Colgan, Daniel McGrath
University of Colorado at Boulder
Cooperative Institute for Research in Environmental Sciences
Campus Box 216, Boulder CO 80309

Manfred Stober, Gerlinde Grom, Susanne Linder
Stuttgart University of Applied Sciences
Department of Surveying and Geoinformatics

NASA Grant NNG06GB08G

Final Progress Report
to
National Aeronautics and Space Administration
March 2009

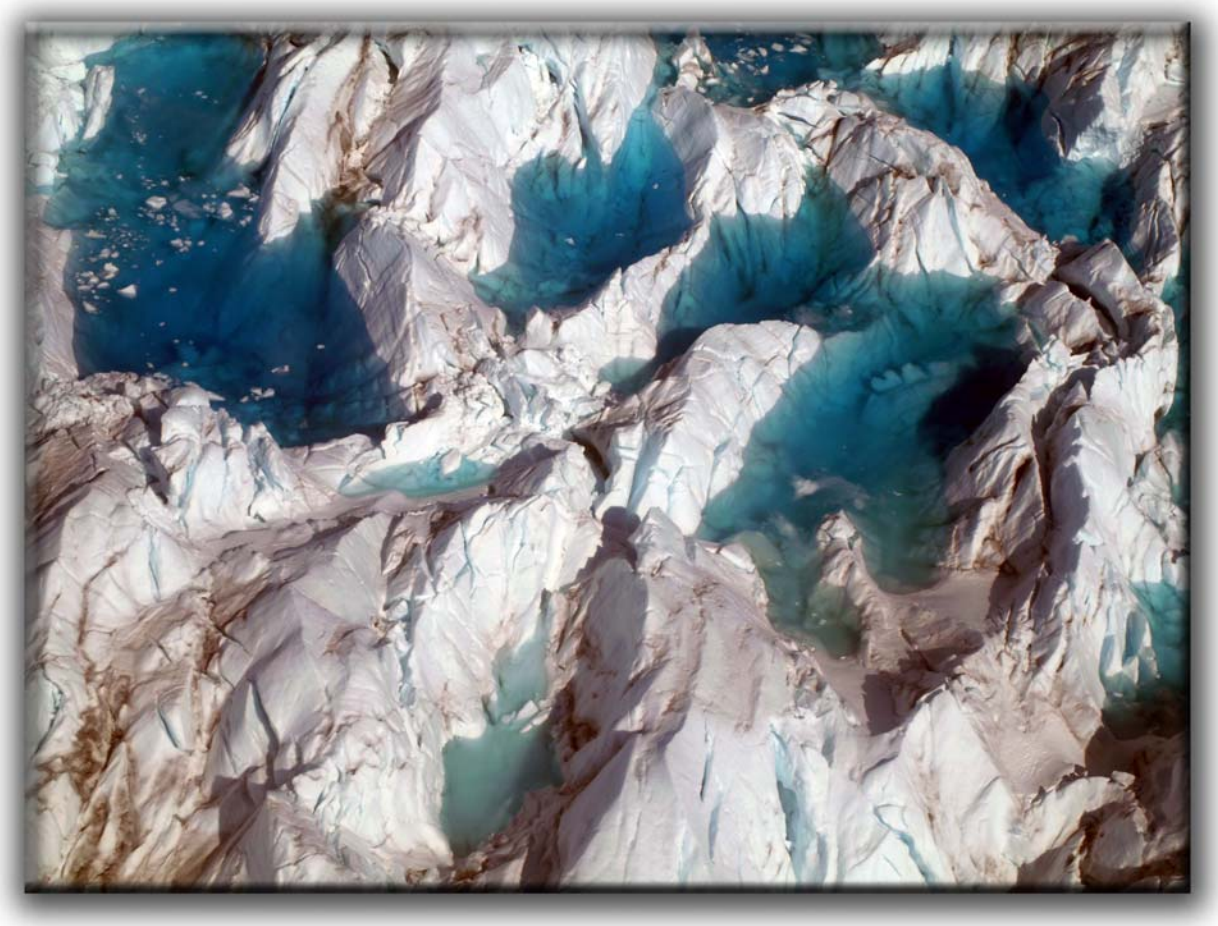

CREVASSES IN LOWER PART OF JAKOBSHAVN ISBRAE FILLED WITH WATER

Table of Content

1. Field Expedition 2008

1.1 Logistic Summary

Date	Location	Work
April 2008		
21	Scotia-SFJ	Team members (Steffen, Philips, Colgan, McGrath) w/C-130
22	SFJ-Qaanaaq	Air Greenland commercial
26	Qaanaaq-Thule	Pick up by Twin Otter and relocate
28	Thule-Pet ELA	AWS download
28	Pet ELA – GITS-Thule	AWS download
28	Thule – Humboldt-Th.	AWS download and extended tower
29	Thule – Tunu N	AWS download, extend tower, 2 nights stay
May 2008		
2	Tunu N- NASA E	AWS download
2	NASA E – Summit	AWS download
2	Summit-NASA U-SFJ	AWS download
3	SFJ-NASA SE	AWS download
3	NASA SE – Saddle	AWS download
3	Saddle – Dye II – SFJ	AWS download
5	SFJ-SC-CP1	Put in to Swiss Camp, AWS download at CP1
5	CP1-N70-SC-SFJ	Could not find N70 GPS and climate station – melted out
8	JAR1	AWS download, re-drilled as station fell over, and melted out
9	JAR2	AWS download and re-drilled
11	Moulin	Download climate data at moulin station
13	Moulin	GPR profiles around moulin
14	SC AWS	Re-drilled tower
16	Moulin	GPR profiles around moulin, install new AWS and GPS
17	Dead Glacier	BBC filming at Dead Glacier
18	SC	Science tower re-drilled
19	S-16	AWS and GPS download
21	SC-Ilulissat	Pull out Steffen and Zwally
June 2008		
2	SC	Swiss Camp pull-out: Phillips, Colgan, McGrath, Sampson

1.2 Automatic Weather Station Maintenance

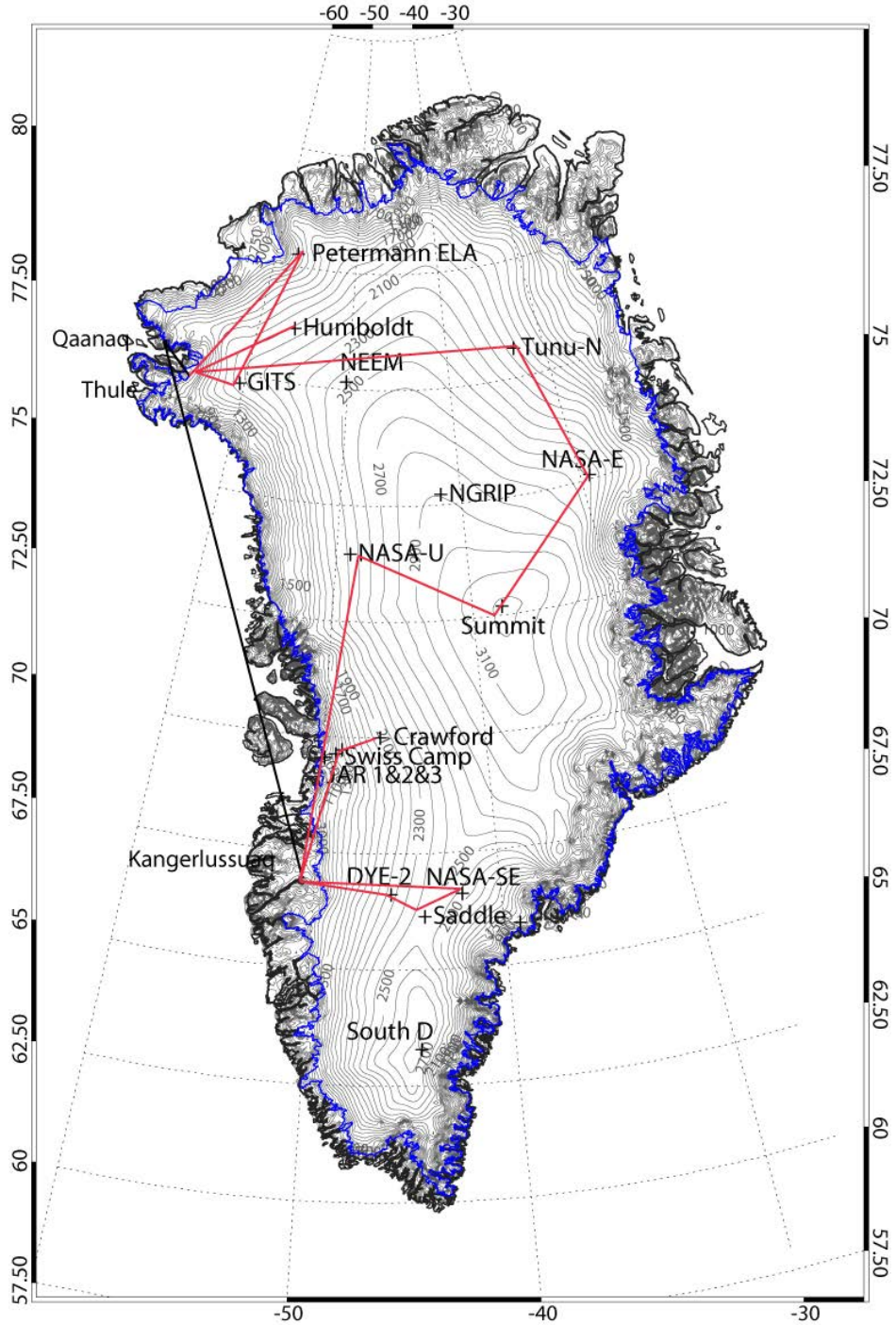

Figure 1.1: Greenland Climate Network (GC-Net) automatic weather stations as of summer 2008. The red arrows indicate the Twin Otter flight path for the AWS maintenance described in the logistic summary.

1.3 Personal

Name	Institution	Arr.	Dep.
AWS support and Swiss Camp research			
Konrad Steffen	CU-Boulder	4/21	5/23
Kevin Sampson	CU-Boulder	4/21	6/2
William Colgan	CU-Boulder	4/21	6/2
Dan McGrath	CU-Boulder	4/21	6/2
Thomas Phillips	CU-Boulder	4/21	6/2
Jay Zwally	NASA-GSFC	5/2	5/23
Alberto Behar	NASA-JPL	5/2	5/12
Moulin Experiment			
Konrad Steffen	CU-Boulder	8/15	8/18
Alberto Behar	NASA-JPL	8/15	8/18
Dan McGrath	Cu-Boulder	8/15	8/18
Seelye Martin	NASA HQ	8/15	8/18
Media Visits			
Patrick Schellenberg	Swiss TV	5/2	5/7
Olivier Dressibourg	Le Temps	5/2	5/7
Mark Binelli	Rolling Stones	5/7	5/12
Olaf Otto Becker	Photographer	5/16	5/25
Marc Christioph	ARD TV	5/24	5/25
Matthias Jung	ARD TV	5/24	5/25
Thomas Schimmock	ARD TV	5/24	5/25

2. Greenland Climate Network (GC-Net)

2.1 Overview

The GC-Net currently consists of 17 automatic weather stations and four smart stakes distributed over the entire Greenland ice sheet (Figure 1.1). Four stations are located along the crest of the ice sheet (2500 to 3200 m elevation range) in a north-south direction, Eight stations are located close to the 2000 m contour line (1830 m to 2500 m), and three stations are positioned in the ablation region (50 m to 800 m), and two stations are located at the equilibrium line altitude at the west coast and in the north.

The GC-Net was established in spring 1995 with the intention of monitoring climatological and glaciological parameters at various locations on the ice sheet over a time period to assess the climate and its variability. The first AWS was installed in 1990 at the Swiss Camp, followed by four AWS in 1995, four in 1996, five in 1997, another four in 1999, one in 2002 one in 2003, and the latest one at NEEM in support for the new deep ice core in 2006. Our objectives for the Greenland weather station (AWS) network are to measure daily, annual and interannual variability in accumulation rate, surface climatology and surface energy balance at selected locations on the ice sheet, and to measure near-surface snow density at the AWS locations for the assessment of snow densification, accumulation, and metamorphosis.

In addition to providing climatological and glaciological observations from the field, further application of the GC-Net data include: the study of the ice sheet melt extent (*Abdalati and Steffen*, 2001); estimates of the ice sheet sublimation rate (*Box and Steffen*, 2001); reconstruction of long-term air temperature time series (*Shuman at al.*, 2001), assessment of surface climate (*Steffen and Box*, 2001), and the interpretation of satellite-derived melt features of the ice sheet (*Nghiem et al.*, 2001). Potential applications for the use of the GC-Net data are: comparison of in-situ and satellite-derived surface parameters, operational weather forecast; validation of climate models; and logistic support for ice camps and Thule AFB.

2.2 GC-Net Users

During the last 12 month we received 91 new GC-Net data requests (61 for 2007) and distributed the data using the new Web interface. The user list is given in the following table. This web interface allows us to capture the email and affiliation of all GC-Net users, including a short description of their use of the Greenland Climate data. The data request is processed on a UNIX 4-processor workstation and the data is transferred on a FTP site for direct downloading. We will continue to maintain the main portal for all GC-Net data distribution, the main raison being the frequent data reprocessing to increase data quality.

ID	Email	Name	Organization
206	460931@swan.ac.uk	Nick Selmes	University of Swansea UK (Glaciology Group
207	koni@seaice.colorado,.edu	koni	UBC
208	Jesper Sjolte	Jesper Sjolte	Nield Bohr Inst. CPH
210	zbzw@amu.edu.pl	Zbigniew Zwolinski	Institute of Paleogeography Adam Mickiewicz
211	bhattacharya.21@osu.edu	indrajit	BPRC, The Ohio State University
212	mary.r.albert@usace.army.mil	Mary Albert	Cold Regions Research & Engineering Lab
213	william.snedjr@maine.edu	Bill Sneed	Univ. of Maine
214	bhattacharya.21@osu.edu	indrajit	osu
215	mail@fengxiao.info	Feng Xiao	CAUC, Civil Aviation Univ. of China
216	barbier_arnaud@yahoo.fr	barbier	
217	kirill.khvorostovsky@nersc.no	Khvorostovsky	NERSC, Bergen, Norway
218	dva@geus.dk	Dirk van As	GEUS
219	s_doutreloup@hotmail.com	Doutreloup Sébastien	
222	eguinaga@gmail.com	Elena Guinaldo	
224	koni@seaice.colorado.edu	koni	
225	clhaman@mail.uh.edu	christine haman	university of Houston
226	joey@ucar.edu	Joey Comeaux	NCAR
227	kimhy@umd.edu	Hye-Yun Kim	University of Maryland
228	rxp245@psu.edu	Rui Peng	Penn State
229	rxp245@psu.edu	Rui Peng	Penn State
230	willismi@gmail.com	Mike Willis	BPRC
231	a.j.sole@bristol.ac.uk	Andrew Sole	University of Bristol, Glaciology Centre
232	rxp245@psu.edu	Rui Peng	Penn State Geography
233	rxp245@psu.edu	Rui Peng	Penn State Geography
234	rxp245@psu.edu	Rui Peng	Penn State Geography
235	rxp245@psu.edu	Rui Peng	Penn State Geography
236	rcampell@pwssc.gen.ak.us	Rob Campbell	Prince William Sound Science Center
237	cornelius.strohm@gmail.com	Cornelius Strohm	private
238	bernalk@mcmaster.ca	Katrina Bernal	McMaster University
239	K.Klauenberg@sheffield.ac.uk	Klauenberg	
241	hkockelkorn@planet.nl	H. Kockelkorn	Museum
242	prasanthi.ishm@gmail.com	prasanthi	
243	sandra@feetofgreen.com	Sandra Halward	Feet of Green
244	K.C.Paxman@sms.ed.ac.uk	Kevin Paxman	Edinburgh University
245	K.C.Paxman@sms.ed.ac.uk	Kevin Paxman	Edinburgh University
246	A.V.Sundal@sms.ed.ac.uk	Aud Sundal	University of Edinburgh
247	lorak@u.washington.edu	Lora Koenig	University of Washington
248	isbel.ramos@usace.army.mil	Isbel Ramos	CRREL
249	rountree@cs.uga.edu	Barry Rountree	University of Georgia
250	isbel.ramos@usace.army.mil	Isbel Ramos	CRREL
251	jack.saba@nasa.gov	Jack Saba	NASA/GSFC

252	aku.riihela@fmi.fi	Aku Riihelä	Finnish Meteorological Institute
253	ywze98@yahoo.com	Wenze Yang	CUNY/Hunter College
254	ColinFay@pdceng.com	Colin Fay	PDC Inc. Engineers
259	tlaepple@awi.de	Laepple	AWI
260	A.V.Sundal@sms.ed.ac.uk	Aud Sundal	University of Edinburgh
261	al3m@bsdmail.org	Hacked by Alemin_Krali	Hacked by Alemin_Krali
262	chapman@atmos.uiuc.edu	John Walsh	University of Illinois at Urbana-Champaign
263	jeff.ridley@metoffice.gov.uk	Jeff Ridley	Met Office Hadley Centre
264	Aud.Sundal@sms.ed.ac.uk	Aud Sundal	University of Edinburgh
265	mpayne@coas.oregonstate.edu	Meredith Payne	Oregon State University
266	asa.rennermalm@gmail.com	Asa Rennermalm	UCLA Department of Geography
267	alexg@ualberta.ca	Alex Gardner	University of Alberta
269	martti.backman@yle.fi	Martti Backman	Finnis Broadcasting Company
270	ehanna@sheffield.ac.uk	Edward Hanna	University of Sheffield
271	kindig@nsidc.org	Dave Kindig	NSIDC
272	emma.j.stone@bristol.ac.uk	Emma Stone	University of Bristol
273	ursula.rick@colorado.edu	Ursula Rick	INSTAAR
274	peyman.rezaei@yahoo.com	Peyman	TU Darmstadt
275	worlali2000@yahoo.com	Eugenia Akpelasi	Personal
276	matthew.shupe@noaa.gov	Matthew Shupe	CIRES
277	gerlindegrom@web.de	Gerlinde Grom	Hochschule Für Technik Stuttgart
278	techs@summitcamp.org	Andy Clarke	NOAA GMD For Summit Station Records
279	neil@uwyo.edu	neil f humphrey	university of Wyoming
280	Ole.Humlum@geo.uio.no	Ole Humlum	University of Oslo
281	dva@geus.dk	Dirk van As	GEUS
282	greuell@knmi.nl	Wouter Greuell	Royal Netherlands Meteorological Institute
283	brian.vasel@noaa.gov	Brian Vasel	NOAA/ESRL
284	nr@space.dtu.dk	Niels Reeh	National Space Institute, Technical University
285	rahvin6@gmail.com	John Robb	Glasgow University
286	cck146@psu.edu	Chris Karmosky	Penn State university
287	N41M4@HOTMAIL.COM	naima ali	queen mary university
288	brandt@atmos.washington.edu	Richard Brandt	Sciences
289	fxsm@uaf.edu	Sebastian H. Mernild	University of Alaska Fairbanks
290	fxsm@uaf.edu	Sebastian H. Mernild	IARC and WERC - University of Alaska Fairbanks
291	s.j.palmer@sms.ed.ac.uk	Steven Palmer	The University of Edinburgh
292	truffer@gi.alaska.edu	Truffer	UAF
293	N41M4@HOTMAIL.COM	naima	
294	N41M4@HOTMAIL.COM	naima	
295	bert.wouters@tudelft.nl	Bert	DEOS - TUDELFT
296	blefer@uh.edu	Barry Lefer	University of Houston
297	shunli@atmosp.physics.utoronto	Shunli Zhang	University of Toronto

2.4 Updated Swiss Camp Climatology

The mean annual temperature has increased by 4.3 ºC using a linear regression model. The minimum temperature in 1992 was the result of the aerosol loading caused by the Mt. Pinatubo eruption. The linear regressing model at 95% confidence shows that the Pinatubo cooling and also the subsequent warming from the mid 90's were outside the 95% level of confidence. The warming that occurred since 2000 to present shows approximately the same trend then the 15-year time series. The warmest mean annual temperature was recorded with -10.3 ºC in 2006. The temperature record for the Swiss Camp 2007 is not available yet but first indications show that it was another record warm year, above all previously recorded values since the beginning of this time series.

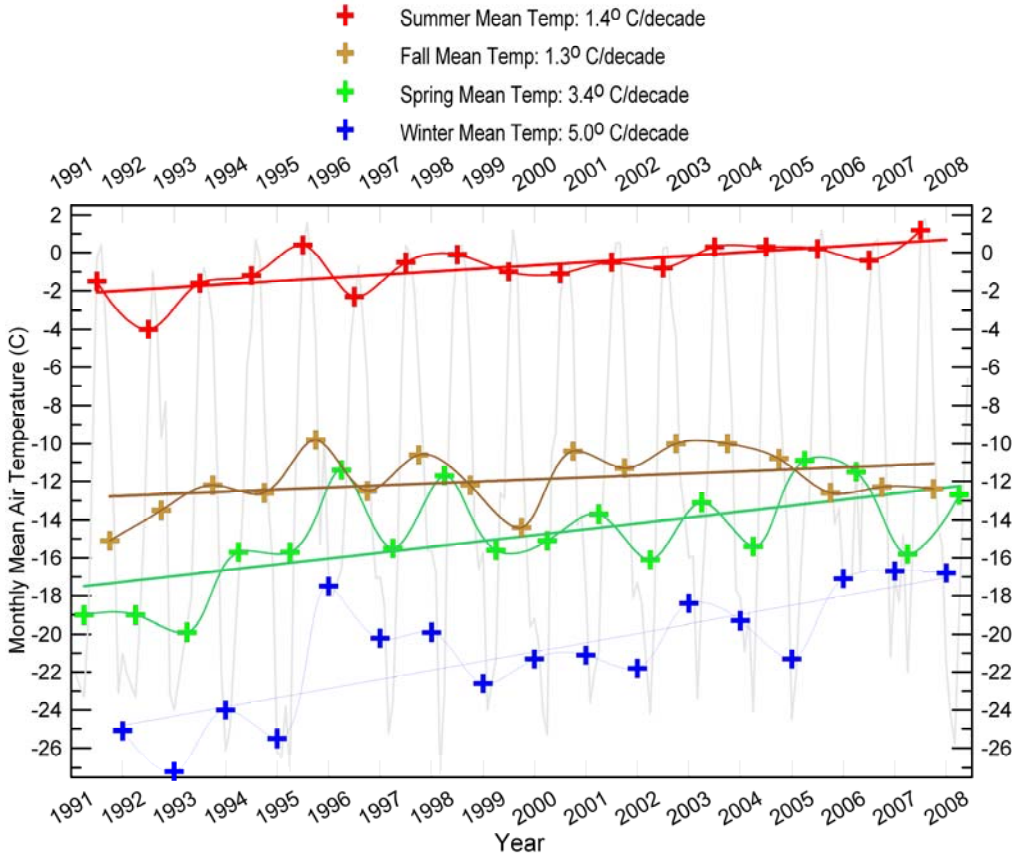

Figure 2.1: Air temperature variability and trend for Swiss Camp, 1991 to 2008.

The statistical analysis of the Swiss Camp air temperature record reveals large interannual variability in all seasons with increasing temperatures throughout the recording period (Fig. 2.1). The mean spring temperature increased 3.4 ºC per decade, and fall temperature increased 1.2 ºC per decade, between 1991 and 2008, using a linear model. The winter temperature showed the largest increase of 5.0 ºC per decade, whereas summer temperatures increased 1.4 ºC per decade during the 18 years (1991 – 2008). The climate record at Swiss Camp shows a clear warming trend that started around 1995, consistent with the Arctic warming.

2.5 Updated Passive Microwave Melt Climatology

The annual melt signal since 1979 is highly variable with a standard deviation that is 28% of the mean (Fig. 2.2). Error bars on the annual total melt area are computed for the first time based on the GC-Net air temperature record. The total melt area in Greenland has increased at a rate of 1.4% per year since 1979 (91% significant.) The melt signal is highly periodic repeating every 3 or 4 years. The record melt year occurred in 2007 and lies 10% above the previous record melt year of 2005. The 1992 melt year, following the Mt. Pinatubo eruption, is the minimum melt year on record at 2 standard deviations below the mean followed closely by 1996 (1.6 standard deviations below the mean.) Peak melt occurs, on average, on August 1st. Increasing trends during July (1.7% per year, 90% significant) and August (1.9% per year, 95% significant) are largely responsible for the overall annual trend (Fig. 2.2). The onset and duration of the melt season have not changed significantly.

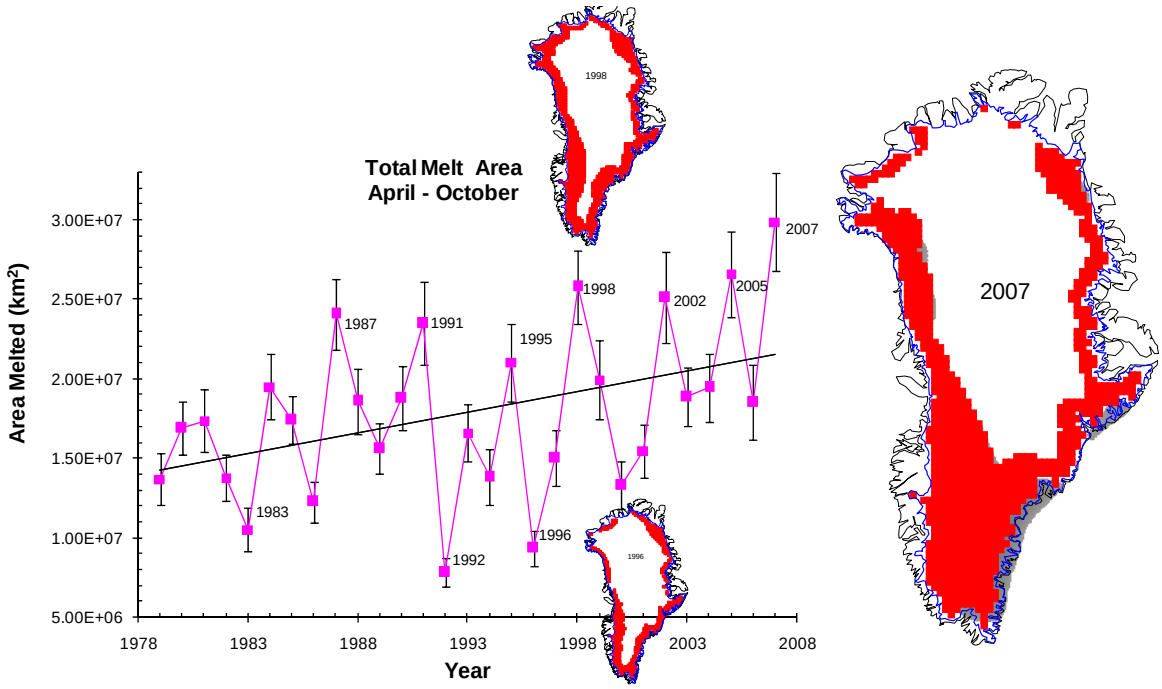

Figure 2.2: Melt climatology for the Greenland ice sheet derived from passive microwave satellite data for 1979 – 2007. Note that the 2007 cumulative annual melt area was 10% higher than the previous record in 2005.

2.5 GC-Net Citation List

This list represents publications that made use of Greenland Climate Network (GC-Net) data.

Abdalati, W. and K. Steffen, Greenland ice sheet melt extent: 1979-1999, J. Geophys. Res., 106(D24), 33,983-33,989, 2001.

Box, J.E., D.H. Bromwich1, B.A. Veenhuis, Le-S. Bai, J.C. Stroeve, J.C. Rogers, K. Steffen, T. Haran, S.-H.. Wang, Greenland ice sheet surface mass balance variability (1988-2004) from calibrated Polar MM5 output, J.Clim., 2005.

Box, J. E., Surface Water Vapor Exchange on the Greenland Ice Sheet Derived from Automated Weather Station Data, PhD Thesis, Department of Geography, University of Colorado, Boulder, CO, Cooperative Institute for Research in Environmental Sciences, 190 pp, 2001.

Box, J.E. and K. Steffen, Sublimation on the Greenland ice sheet from automated weather station observations, J. Geophys. Res., 106(D24), 33,965-33,982, 2001.

Bromwhich, D., J. Cassano, T. Klein, G. Heinemann, K. Hines, K. Steffen and J. Box, Mesoscale modeling of katabatic winds over Greenland with Polar MM5, Mon. Weather Review, 129, 2290-2309, 2001.

Cassano, J.J., J.E. Box, D.H. Bromwich, L. Li, and K. Steffen, Evaluation of Polar MM5 simulations of Greenland's atmospheric circulation, J. Geophys. Res., 106(D24), 33,867-33,890, 2001.

Cullen, N., and K. Steffen, Unstable near-surface boundary conditions in summer on top of the Greenland ice sheet., Geophys. Res. Lett., 28(23), 4491-4494, 2001.

Cullen, N.J., K. Steffen, and P. D Blanken, Nonstationarity of Turbulent Heat Fluxes at Summit, Greenland, Boundary-Layer Meteorology, DOI 10.1007/s10546-006-9112-2, 2006.

Davis, C.H. and D.M. Segura, An algorithm for time-series analysis of ice sheet surface elevations from satellite altimetry, IEEE Transactions on Geoscience & Remote Sensing, 39(1), 202-206, 2001.

Dassau, T.M., A. Sumer, S. Koeniger, P. Shepson, J. Yang, R. Honrath, N. Culen, K. Steffen, Investigation of the role of the snowpack on atmospheric formaldehyde chemistry at Summit, Greenland, J. Geophys. Res., 107(D19), ACH 9.1-14, 36, 2595-2608, 2002.

Hall, D.K., J.E. Box, K.A. Casey, S.J. Hook, C.A. Shuman and K. Steffen, Comparison of satellite-derived and in-situ observations of ice and snow surface temperatures over Greenland, *Remote Sensing of the Environment*, 112(10), 3739-3749, 2008.

Hanna , E., P. Huybrechts, K. Steffen, J. Cappelen, R. Huff, Ch. Shuman, T. Irvine-Fynn, S. Wise, and M. Griffiths. Increased runoff from melt from the Greenland Ice Sheet: a response to global warming. *J. Climate*, 21, 331-341, DOI: 10.1175/2007JCLI1964.1, 2008.

Hanna,H., P.Huybrechts, I. Janssens, J..Cappelen, K. Steffen, and A. Stephens, Runoff and mass balance of the Greenland ice sheet: 1958–2003, J. Geophys. Res., 110, D13108, doi:10.1029/2004JD005641, 2005.

Hanna, E. and P. Valdes, Validation of ECMWF (re)analysis surface climate data, 1979-1998, for Greenland and implications for mass balance modeling of the Ice Sheet, Intern. J. Clim., 21, 171-195, 2001.

Helmig, D, J. Boulter, D. David, J. Birk, N. Cullen, K. Steffen, B. Johsnon, S. Oltmans, Ozone and meteorological boundary-layer conditions at Summit, Greenland, Atm. Environm., 36, 2595-2608, 2002.

Herzfeld, U.C., J.E. Box, K. Steffen, H. Mayer, N. Caine, and M. Losleben, A case study on the influence of snow and ice surface roughness on melt energy, Zeitschrift für Gletscherkunde und Glazialgeology, 39, 1-42, 2006.

Honrath, R.E. Y.Y. Lu, M.C. Peterson, J.E. Dibb, M.A. Arseault, N.J. Cullen, and K. Steffen. Vertical fluxes of NOx, HONO, and HNO3 above the snowpack at Summit, Greenland. Atm. Environm, 36, 2629-2640, 2002.

Klein, T., G. Heinemann, D. H. Bromwich, J. J. Cassano and K. M. Hines, Mesoscale modeling of katabatic winds over Greenland and comparisons with AWS and aircraft data, J. Met. Atmos. Phys., 8(1/2), 115-132, 2001.

Klein, T., G. Heinemann, Simulations of the katabatic wind over the Greenland ice sheet with a 3D model for one winter month and two spring months, Report of the DAAD/NSF project 315-PP, 1999.

Mernild, S.D., G.E. Liston, C.A., Hiemstra, C.A., and K. Steffen, Record 2007 Greenland ice sheet surface melt extent and runoff, *EOS*, 90, 13-14, (Jan 13), 2009.

Mernild, S., G. Liston, Ch. Hiemstra, K. Steffen, E. Hanna, and J.H. Christensen, Greenland Ice Sheet surface mass-balance modeling and freshwater flux for 2007, and in a 1995–2007 perspective. *J. Hydrometeorology*, 9, DOI: 10.1175/2008JHM957.1, 2008.

Mernild, S., G. Liston, Ch. Hiemstra, and K. Steffen. Surface melt area and water balance modeling on the Greenland ice sheet 1995-2005. Geophys. Res. Lett., in press 2007.

Mosley-Thompson, E., J.R. McConnell, R.C. Bales, Z. Li, P.-N. Lin, K. Steffen, L.G. Thompson, R. Edwards, D. Bathke, Local to regional-scale variability of annual net accumulation on the Greenland ice sheet from PARCA cores, J. Geophys. Res., 106 (D24), 33,839-33852, 2001.

Murphy, B. F., I. Marsiat and P. Valdes, Simulated atmospheric contributions to the surface mass balance of Greenland. J. Geophys. Res., 106, submitted, 2001.

Nghiem, S.V., , K. Steffen, G. Neumann, and R. Huff, Snow Accumulation and Snowmelt Monitoring in Greenland and Antarctica, International Association of Geodesy Publication, Dynamic Planet , Chapter 5, 31-38, 2007.

Nghiem,S,V., K. Steffen, G. Neumann, and R. Huff, Mapping of ice layer extent and snow accumulation in the percolation zone of the Greenland ice sheet, J. Geophys., Res., 110, F02017, doi:10.1029/2004JF000234, 2005.

Nghiem, S.V., K. Steffen, R. Kwok, and W.Y. Tsai, Diurnal variations of melt regions on the Greenland ice sheet, J. Glaciol., 47(159), 539-547, 2001.

Nolin, A. and J. Stroeve, The Changing Albedo of the Greenland Ice Sheet: Implications for Climate Change, Annals of Glaciology, 25, 51-57, 1997.

Orr, A., E. Hanna, J. Hunt, J. Cappelen, K. Steffen and A. Stephens, Characteristics of stable flow over southern Greenland, *Pure and Applied Geophysics* (PAGEOPH), 161(7), 2004.

Painter, T.H., N.P. Molotch, M. Cassidy, M. Flanner, and K. Steffen, Contact spectroscopy for determination of stratigraphy of snow grain size, *J. Glaciol*, 53(180) 121-127, 2007.

Parry, V., P. Mair, J. Scott, B. Hubbard, K. Steffen, and D. Wingham, Investigations of meltwater refreezing and density variations in the snowpack and firn within the percolation zone of the Greenland Ice Sheet, Ann. Glaciol., 46, 621-68, 2007.

Rial., J., C. Tang, and K. Steffen, Glacial Rumblings from Greenland's Jakobshavn Ice Stream, *J. Glaciolo*., in press, 2009.

Serreze, M., J. Key, J. Box, J. Maslanik, and K. Steffen, A new monthly climatology of global radiation for the Arctic and comparison with NCEP-NCAR reanalysis and ISCCP-C2 field, J. Climate, 11, 121-136, 1998.

Shuman, C., K. Steffen, J. Box, and C. Stearn, A dozen years of temperature observations at the Summit: Central Greenland automatic weather stations 1987-1999, J. Appl. Meteorol., 40(4),741-752, 2001.

Smith, L.C., Y. Sheng, R.R. Foster, K. Steffen, K.E. Frey, and D.E. Alsdorf, Melting of small Arctic ice caps observed from ERS scatterometer time series, Geophys. Res. Lett., 30(20), CRY 2-14, 2003.

Steffen, K., S.V. Nghiem, R. Huff, and G. Neumann, The melt anomaly of 2002 on the Greenland Ice Sheet from active and passive microwave satellite observations, Geophys. Res. Lett., 31(20), L2040210.1029/2004GL020444, 2004.

Steffen, K., and J.E. Box, Surface climatology of the Greenland ice sheet: Greenland climate network 1995-1999, J. Geophys. Res., 106(D24), 33,951-33,964, 2001.

Steffen, K., W. Abdalati, and I. Serjal, Hoar development on the Greenland ice sheet, J. of Glaciology, 45(148), 63-68, 1999.

Steffen, K., J. E. Box and W. Abdalati, Greenland climate network: GC-Net, CRREL, 98-103 pp., 1996.

Stroeve, J., Assessment of Greenland Albedo Variability from the AVHRR Polar Pathfinder Data Set, J. Geophys. Res., 106(D24), 33,989-34,006, 2001.

Stroeve, J., and A. Nolin, 1997. The changing albedo of the Greenland ice sheet: implications for climate modeling, Ann. of Glaciol., 25, 51-57.

Stroeve, J, J. E. Box, J. Maslanik, J. Key, C. Fowler, Intercomparison between in situ and AVHRR Polar Pathfinder-derived surface albedo over Greenland, Remote Sensing of the Environment, 75(3), 360-374, 2001.

Thomas, R., and PARCA instigators, Program for Arctic Regional Climate Assessment (PARCA): Goals, key findings, and future directions, J. Geophys. Res., 106(D24), 33,691-33706, 2001.

Thomas, R.H., W. Abdalati, E. Frederick, W.B. Krabill, S. Manizade, and K. Steffen, Investigation of surface melting and dynamic thinning on Jakobshavn Isbrea, Greenland, J. Glaciol., 49(165), 231-239, 2003.

Wang, L., M. Sharp, B. Rivard, and K. Steffen, Melt duration and ice layer formation on the Greenland ice sheet, 2000-2004, J. Geophys. Res., 112, F04013, doi:10.1029/2007JF000760 2007.

Zwally, H.J. W. Abdalati, T. Herring, K. Larsen, J. Saba, and K. Steffen. Surface melt-induced acceleration of Greenland ice-sheet flow, Science, 297, 218-222, 2002.

3. Results

3.1 Melt Water and Ice Sheet Dynamics

3.1.1 Importance of water in ice dynamics

Glaciohydrology may have also been a key contributor to the eventual demise of the Scandinavian ice sheet (*Arnold and Sharp*, 2002). As a result of concerns over contemporary sea level rise and ice sheet stability, the influence of meltwater on the ice dynamics of the Greenland Ice Sheet is a highly topical branch of cryospheric research. The velocity at which a glacier flows is the product of three distinct physical mechanisms: (i) internal deformation, (ii) basal slide and (iii) basal sediment deformation (Figure 3.1.1). Increased surface meltwater production may potentially enhance each of these three processes on varying time-scales.

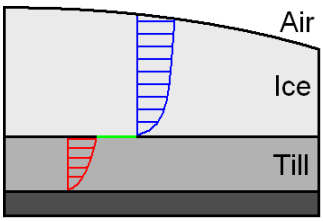

Figure 3.1.1: Schematic of the three mechanisms by which ice flows: internal deformation (blue), basal slide (green) and basal sediment deformation (red). Increased surface meltwater production can enhance each of the three mechanisms.

The internal deformation of ice is best described as a non-linear viscosity-dependent power law ($n \approx 3$) relation between strain rate and stress (*Marshall*, 2005). The effective viscosity of ice is highly temperature dependent, varying between 10^{11} and 10^{17} Pa s over the temperature range of -2 to -32 °C in the Greenland Ice Sheet (*Marshall*, 2005). As the surface meltwater production of the Greenland Ice Sheet increases, moulin discharge into the englacial system can be expected to increase as well. Over long time scales, increased englacial water may sufficiently warm marginal portions of the Greenland Ice Sheet to significantly decrease their effective viscosity.

Increases in surface meltwater production may also be expected to lead to increases in subglacial water pressure (*Zwally et al.*, 2002). Basal sediment deformation increases with increased subglacial water pressure. Increased pore water pressure decreases the shear strength of failure of sediment, which results in increased ice flow (*Tulaczyk et al.*, 2000). Basal sediment deformation only occurs when sufficient subglacial till is present. It is not known whether rates of basal sediment deformation vary on relatively long or short time-scales. In ice caps and ice sheets, however, the contribution of basal sediment deformation to ice flow is likely negligible in comparison to the components of internal deformation and basal slide (*Marshall et al.*, 2005).

Basal slide occurs when increases in subglacial water pressure reduce basal friction by making a portion of the overburden ice column buoyant. As the floatation fraction of the overlying ice increases, friction decreases and ice flow increases (*Flowers and Clarke*, 2002). The relation between subglacial water volume and basal slide is not entirely clear, as different subglacial hydrological configurations (i.e. ice-walled conduits, bedrock conduits, water film, linked cavities, soft-sediment channels, porous sediment sheets and ordinary aquifers) result in different water pressures for a given water volume (*Flowers and Clarke*, 2002). Unlike the other two mechanisms of ice flow, however, basal slide can constitute a substantial portion of total ice flow and responds to changes in subglacial water pressure on short time-scales (*Zwally et al.*, 2002).

3.1.2 The relation between surface melt and basal slide

Previous PARCA-funded research has found ice flow in west-central Greenland to accelerate during periods of summer melting and decelerate after melt cessation. The apparent relation between ice acceleration and the duration of summer melting has been interpreted as evidence of enhanced basal slide due to the rapid channeling of surface meltwater to the bed during melt periods (*Zwally et al.*, 2002; Figure 3.1.2). Naturally, the presence of subglacial water requires warm-based conditions. Recent coarse-resolution modeling suggests that the majority of the marginal area of the Greenland Ice Sheet is indeed warm-based (*Marshall*, 2005). As the surface melt in the marginal areas of the Greenland Ice Sheet increases beyond long term equilibrium (*Hanna et al.*, 2008), a greater volume of surface meltwater may be expected to reach the subglacial system in marginal areas. This would be expected to increase the floatation fraction, and enhance basal slide, in the marginal areas of the Greenland Ice Sheet.

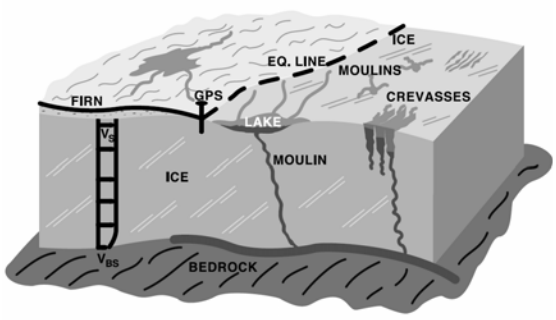

Figure 3.1.2: Schematic illustrating the routing of surface meltwater to the subglacial system (*Zwally et al.*, 2002)*. Increased subglacial water pressure can enhance basal slide.*

A well-constrained 2D (*x,y*; depth-integrated) model of high spatial and temporal resolution (the Swiss Camp regional model) is under development at the Cooperative Institute for Research in Environmental Science (CIRES) at the University of Colorado by a PhD candidate (William Colgan) under the supervision of Dr. Konrad Steffen. In addition to forecasting both short and long-term regional sea level rise contributions, this model aims to (i) assess the present spatial distribution of warm-based ice in the Jakobshavn region by modeling the standard heat equation terms (advection, diffusion and production) with specified ice temperature boundary conditions. The model will (ii) investigate the physical basis of the relation between increased surface melt and enhanced basal slide. It is important to be able to predict how the magnitude and/or spatial distribution of this phenomenon may evolve in the next century. Finally, the model will (iii) determine the stable ice margin configuration of Jakobshavn Isbrae by assessing the stability of the current grounding line to perturbations.

3.1.3 The Swiss Camp regional model

A 1D (*x*) thermodynamic glacier model has been developed at CIRES as a precursor to the 2D (*x,y*) Swiss Camp regional model. The 1D model is also depth-integrated, meaning that it ignores vertical ice flow in the *z*-direction. Previous work has shown this to be a reasonable approximation (*Marshall et al.*, 2005; Ice flow in the *z*-direction is, however, used to calculate heat advection terms). Longitudinal coupling is explicitly addressed in the model (*van der Veen*, 1987). Longitudinal coupling is the “pushing” or “pulling” of an ice column against its neighbor. This process is important in areas with complex bed topography (i.e. reverse slopes) and shallow ice. Previous work has suggested that the enhanced basal slide mechanism observed near Swiss Camp may actually occur some distance downstream from Swiss Camp, with the enhanced ice flow signal being propagated upstream through longitudinal coupling (*Price et al.*, 2008). The bedrock topography is known to be very complex in the vicinity of Swiss Camp (*Plummer et al.*, 2008). The 1D longitudinally coupled ice dynamic model has proved capable of treating ice flow over idealized complex bed to-

pography which has an icefall that exceeds ice thickness (Figure 3.1.3). This 1D longitudinally coupled ice dynamic model is now being tested with observed bed topography data along flowlines in the Swiss Camp region.

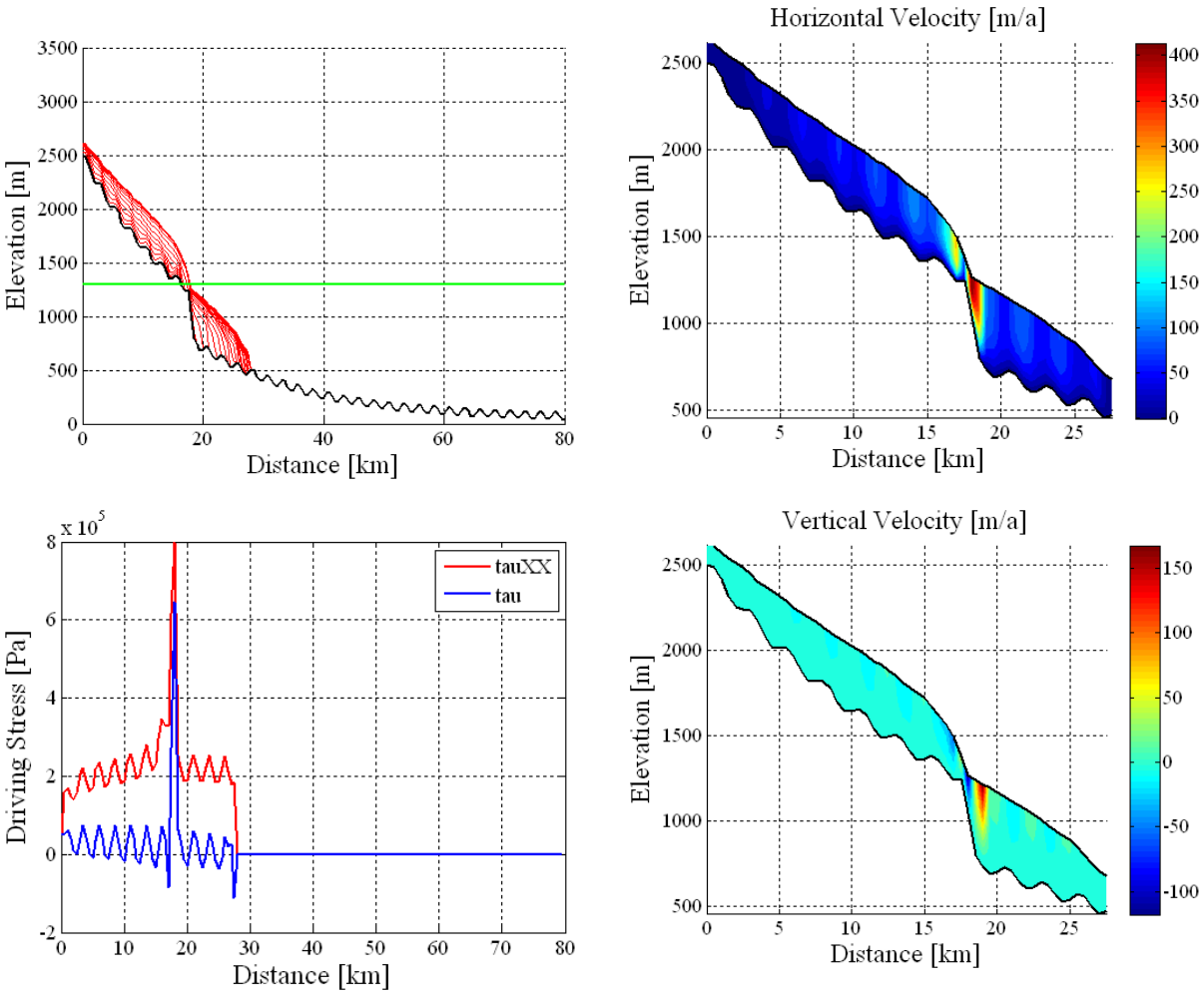

Figure 3.1.3: Sequentia time-steps of the 1D longitudinally coupled ice dynamic model initialized with idealized complex bed topography that has an icefall which exceeds ice thickness at x = 18 km (**top left**; *equilibrium line altitude in green). Longitudinal coupling stress* (tauXX) *and total driving stress* (tau) *along the glacier profile* (**bottom left**), *horizontal* (**top right**) *and vertical velocity* (**bottom right**) *with depth along the glacier profile are also shown at the final time-step.*

As ice flow is highly dependent on effective viscosity, which is in turn highly dependent on ice temperature, the 1D- longitudinally coupled ice dynamic model is coupled to a 2D (*x*,*z*) heat equation model. The heat equation model calculates the temperature at 20 vertical levels within the ice. Prescribed boundary conditions of surface and bed ice temperatures are used to calculate diffusion terms, while 2D (*x*,*z*) velocity components are used to calculate advection terms. Finally, heat production terms (due to the heat released by internal deformation) are calculated using the total driving stress at each node. As changes in ice temperature occur on relatively long time-scales, in comparison to changes in ice geometry, the 2D heat equation model only updates ice temperatures and effective viscosities in the 1D dynamic model every 10 years. The 1D dynamic model is currently being run at 0.01 year time-steps. This time-step can be further reduced once a hydrology model with diurnal variations in surface meltwater production has been incorporated. The 1D flowline model with coupled ice dynamics, ice temperature and hydrology is scheduled for completion in March 2009.

Once the 1D model has been validated, and predictions made along a flowline, the model will be modified into a 2D (*x*,*y*) depth-integrated model which will also be validated. The models will be validated using observed surface ice velocity data collected both in-situ (*Zwally et al.*, 2002) and remotely (*Rignot and Kanagaratnam*, 2006) by previous PARCA-funded investigations. The 2D Swiss Camp regional model has a domain that extends ~110 km north-south (68.7 to 69.7 °N) and ~300 km east-west (43.5 to 51.0 °W). This domain includes both Swiss Camp and the terminal portion of the Jakobshavn Isbrae drainage basin, the largest drainage basin of the Greenland Ice Sheet (Figure 3.1.4). With an anticipated grid size of 500 x 500 m, and with 20 vertical levels in the ice, we expect to solve approximately 2.6 million degrees of freedom in each time step (where "degrees of freedom" is the product of the number of *x*-nodes, *y*-nodes and *z*-nodes). This computation is feasible at a 0.001 to 0.01 year time-step with efficient numerical methods.

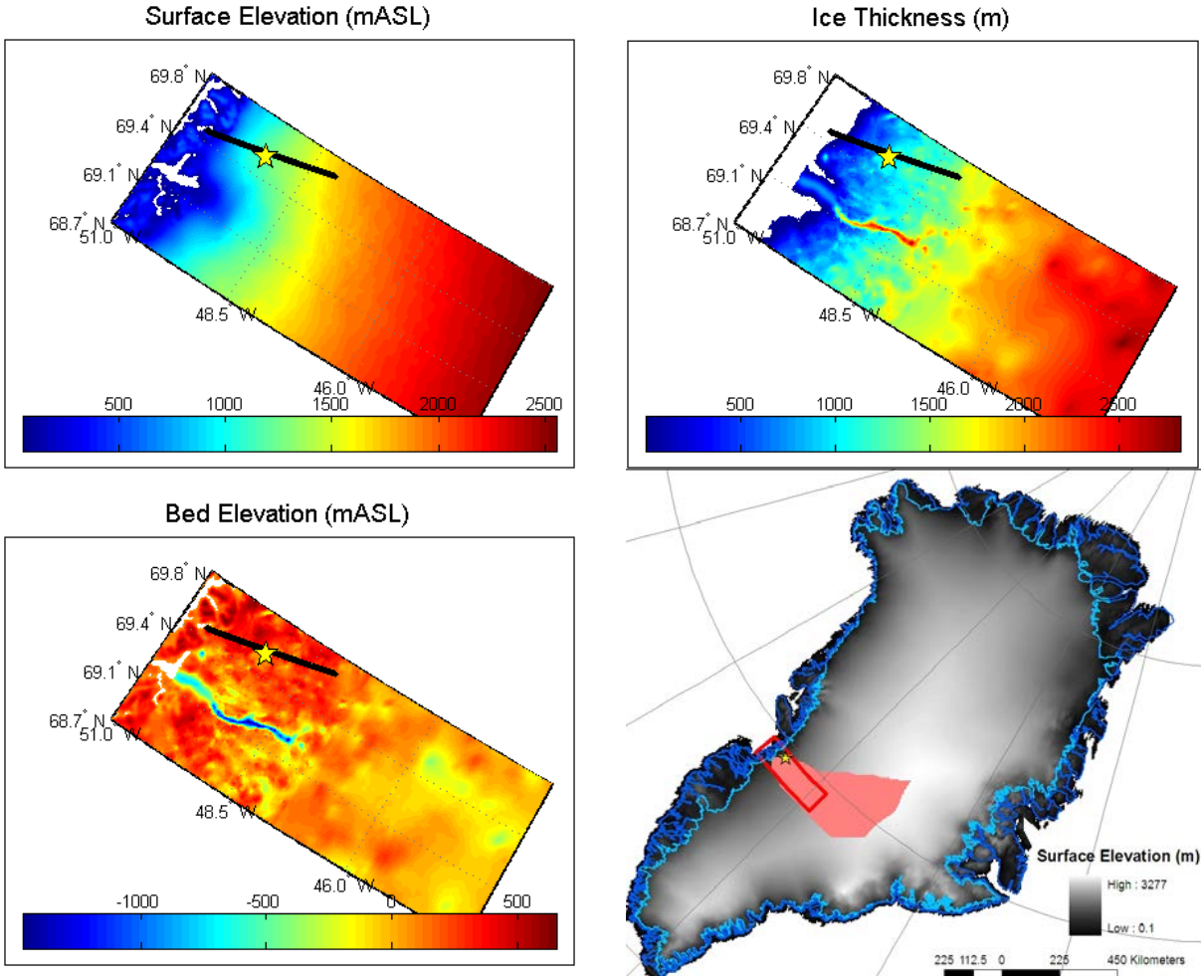

Figure 3.1.4: The Swiss Camp regional model: ice surface elevation (**top left**)*, ice thickness* (**top right**)*, bedrock elevation* (**bottom left**) *and the location of the model domain within the Jakobshavn drainage basin (red shading) in Greenland* (**bottom right**)*. Swiss Camp is marked with the star, while the black line is the flowline currently under consideration (after Price et al.,* 2008*).*

The Swiss Camp regional model is initialized with both geometry and climatology datasets. The geometry datasets drive the ice dynamic portion of the model and come from a variety of previous PARCA-funded projects. The ice surface topography was interpolated from a 625 m digital elevation model (DEM) constructed from Advanced Very High Resolution Radiometer (AVHRR) satel-

lite images that were further enhanced by photoclinometry (*Scambos and Haran*, 2002; Figure 3.1.4). The ice thickness data used in the Swiss Camp regional model is interpolated from two sources: (i) a recently acquired 150 m ice thickness DEM derived from airborne ice-penetrating radar west of 47.5 °W (*Plummer et al.*, 2008), and (ii) an older 2 km ice thickness DEM also derived from airborne ice-penetrating radar east of 47.5 °W (*Bamber et al.*, 2001). The climatology datasets drive the ice temperature and surface mass balance portion of the model. The Swiss Camp regional model will use an evolving mass balance model in which the surface balance of each grid cell is dependent on latitude, longitude and elevation. Surface climatology will likely be drawn from a reanalysis dataset (i.e. Japanese 25-year Reanalysis Project) and validated with previously collected climatology datasets (*Box and Steffen*, 2001).

The 2D hydrology model is the most challenging aspect of the Swiss Camp regional model. Currently, the 2D hydrology model assumes that the spatial distribution of subglacial meltwater input is dependent on the spatial distribution of perennial moulins (moulins with deeply incised supra-glacial drainage systems). The spatial distribution of moulins can be expressed as a moulin density in each grid cell. Analysis of observed moulin locations (*Thomsen et al.*, 1985) has found moulin density to range between 0 and 0.88 km^{-2} (Figure 3.1.5). This corresponds to a minimum moulin catchment area of 1.13 km^2. Initial efforts to model this observed moulin density using six independent variables (positive degree days, ice surface slope, bedrock slope, ice driving stress, ice velocity and crevasse presence) have been successful in reproducing approximately half of the variance ($r^2 \approx 0.5$; standard error < 0.1 km^{-2}) in observed moulin density across a sub-region of the Swiss Camp regional model domain. Field experiments in the vicinity of Swiss Camp are being used to estimate moulin discharge. Further refinement of the moulin density model and assumptions about the portion of moulin discharge which reaches the bed can be combined with a subglacial hydrological routing model, driven by pressure-gradients, to give a reasonable approximation of the subglacial water pressure throughout the Swiss Camp regional model domain.

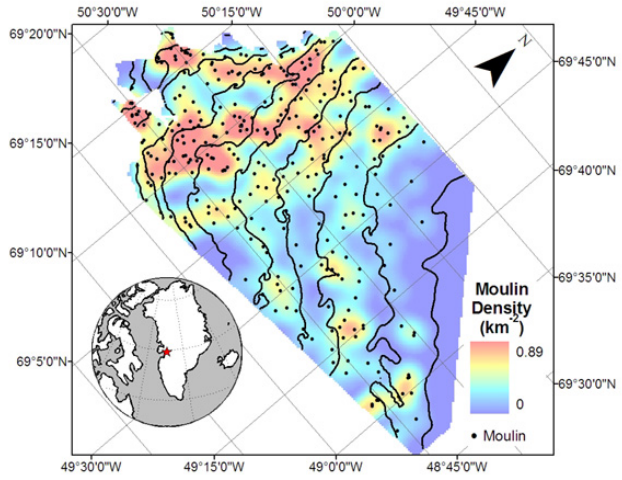

Figure 3.1.5: The observed moulin density, in a sub-region of the Swiss Camp model domain, calculated from observed moulin locations (points; Thomsen et al., 1985*). The contour interval is 100m.*

The relatively high quality of datasets previously collected in the Swiss Camp region make it a unique area in which to construct a well constrained model of high spatial and temporal resolution that can predict the effects of projected future increases in surface meltwater production on the ice dynamics of this region. The 2D Swiss Camp regional model is scheduled for completion in the fall of 2009. The model will provide predictive capabilities to: (i) assess the present and future extent of warm-based ice in the Jakobshavn region, (ii) quantify the magnitude and spatial distribution of the relation between increased surface melt and enhanced basal slide, and (iii) assess the stable ice margin configuration of Jakobshavn Isbrae. The intent is to give the model sufficient flexibility so

as to allow the possibility of using entire ice sheet climatology and geometry should computational resources become available in the future.

3.2 Ice Temperatures

The University of Colorado has been carrying out a moulin experiment since 2006. The aim of this study is to get a better understanding of the melt patterns in Western Greenland and the relevance of the melt volume on the annual en-glacial hydraulic system as well as on basal lubrication and the resulting increase in the outlet glaciers' velocities. Embedded in the project is a study to model the response of the ice sheets thermal household to different forcing such as shear stress, heat conduction and more importantly of the possible impacts of en-glacial water. In a first step four minor sensitivity studies using automatic weather station data (AWS hereafter) from the nearby Jakobshavn Ablation Region station 1 (JAR1 hereafter) were carried out as pilot projects. These for pilot studies included:

- Statistical analysis of the dependency of measured ice temperatures in the first 10m on the overlaying snow cover and the temperature of the atmosphere.
- A one dimensional partial differential heat diffusivity model is used to analyze the diurnal temperature patterns at various ice depths.
- A one dimensional partial differential advection-conduction model was programmed to simulate the impact of snow and atmospheric variability on ice temperature as well as the en-glacial temperature household.
- Melt rates for different months were analyzed for spatial and temporal resolution using AWS data and MODIS Terra images.

The data used is from the Greenland Climate Network station JAR1 which is located in western Greenland approximately 70 km inland from Ilulissat and north of the Jakobshavn glacier. It is located on the Dead Glacier (Figure 3.2.1, right) at 69°29'54"N, 49°40'54"W and at an elevation of 972m a MSL. The data used in these studies included 4 channels of atmospheric near surface temperature as well as 10 channels of thermocouple ice temperature measurements for 1 meter through 10 meters depth. In addition two channels for relative snow height change were used to calculate the snow depth and the melt volume.

In addition an experiment at the Moulin was carried out from May through August 2008 to analyze the behavior of en-glacial ice temperature while it is melting out. Thermistors were used to measure the temperature curves. At the start of the experiment the thermistors were set at depths 25 cm, 50 cm, 75 cm, 1 m and 4.5 m bellow the ice surface. The snow cover was 1.52 m thick at that point. The graphs have so far only been analyzed in a qualitative fashion but will be used in order to understand the phase change of ice to water better and increase the accuracy of modeling the process.

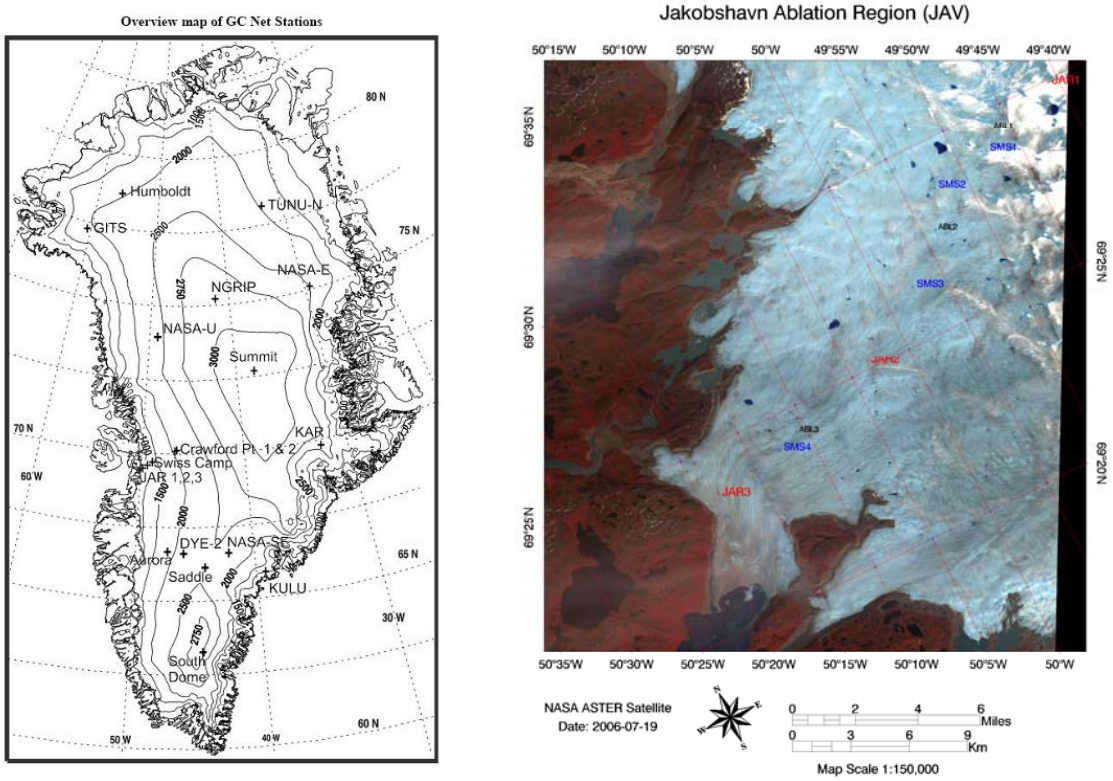

Figure 3.2.1: The study area located in western Greenland, north of the world's fastest moving glacier the Ilulissat Glacier. In the image on the left the exact location of JAR1 is to be found.

3.2.1 Statistical analysis of ice temperature behaviour

A statistical analysis using cross correlation was used to study the behavior of the dependent ice temperature on the snow cover thickness at the surface. Monthly averages were used for the years 1997 through 2002. The analysis showed that there is a significant correlation between the snow cover thicknesses above the 95 percentile for each depth. The lag time varies from zero for 1 meter depth to approximately 6 months at 10 meters depth. The lag time can be viewed in Table 3.2.1.

Depth	Time Lapse	Depth	Time Lapse
1 meter	0 months	6 meters	3 & 4 months
2 meters	0 months	7 meters	4 months
3 meters	1 months	8 meters	4 months
4 meters	2 months	9 meters	6 months
5 meters	2 months	10 meters	6 months

Table 3.2.1: The calculated time lag of the temperature response at each ice depth correlated to the surface snow height. The correlation for each depth is above the 95% percentile.

In a second analysis the correlation for the mean monthly ice temperatures to the atmospheric temperatures for different seasons was calculated and compared to the correlation for the whole season. The correlation for the months May through December which have little snow is significantly correlated above the 95% percentile for temperatures as far as 5 meters into the ice. The same analyses for all year data showed a lower correlation coefficient or each depth and bellow the 95% percentile for temperatures at 3 meters depth. The results can be viewed in Table 3.2.2.

	Dept 1m	Depth 2m	Depth 3m	Depth 4m	Depth 5m
All year	99.5	98.7	94.9	90.0	84.0
May -Dec	99.6	99.9	98.7	97.8	95.7

Table 3.2.2: The correlation coefficients for the correlation analysis including all 12 months of the year. Second row: The correlation coefficients including only the months with no or little snow cover.

3.2.2 One dimensional diffusivity model

The signature of the diurnal variability on the course of the en-glacial temperature is modeled. The Fourier equation for heat conduction is used. The physical properties for ice are set to 2000J/Kg/K for the heat capacity, 2.1 W/m/K for the heat conduction and 917 kg m^3 for the ice density. The diffusivity term is $1.145e^{-6}$.

In this theoretical approach the initial ice condition is taken as being at -5 Celsius. The surface boundary condition is the air temperature which is oscillating over 24 hours with amplitude of 10 Celsius and a mean temperature of -5 Celsius. The temperature curve at various depths is analyzed. In the following Figure 3.2.2 the daily amplitude including lapse time may be seen in the left figure. In the right figure the daily temperature profile for 24 hours and 2 meters depth with no snow cover is plotted.

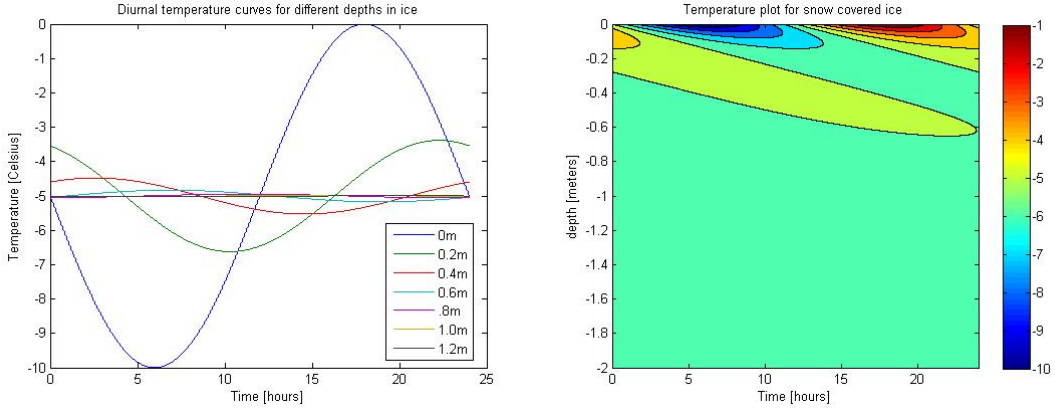

Figure 3.2.3: The influence of the air temperature on the ice temperature for the first 2 meters below the surface. On the left are diurnal curves for different depths; on the right is a time plot for the temperature profile for the first 2 meters of ice.

At a depth of 45 cm the diurnal temperature curve shows 10% of the amplitude at the surface. At 80 cm depth a diurnal cycle of 0.2 deg Celsius is calculated. A fast Fourier Transformation analysis showed no significant 24 hour repetitive cycle at 1 meter depth which supports our finding.

During the 2008 melt season the ice temperature just below the surface was measured using thermistors. On day 137 when they were put in they were located at depths of 25, 50, 75 and 100 cm as well as at 4.5 m. There was snow cover of 152 cm thickness. The first 14 days show similar resistance measurements for all depths. This is considered to be the initializing period. The raw data in Figure 3.2.4 shows the upper 4 thermistors measuring a similar increase in temperature over time but with different absolute values. The measurement at 4.5 m has a less steep increase over time. On day the blue and the black plot show an oscillation setting in. The wavelength is approximately 24 and is recognized as a diurnal signal. All four shallow thermistors reach an ice thermistor value where no increasing trend remains. This may be when the temperature reaches the melting point. Later in the plot the diurnal amplitudes increase and are assumed to be the atmospheric signal and the result of the thermistor being melted out. The data will be analyzed for temperature and for depth below the surface and in a follow up study this data will be used to validate the model.

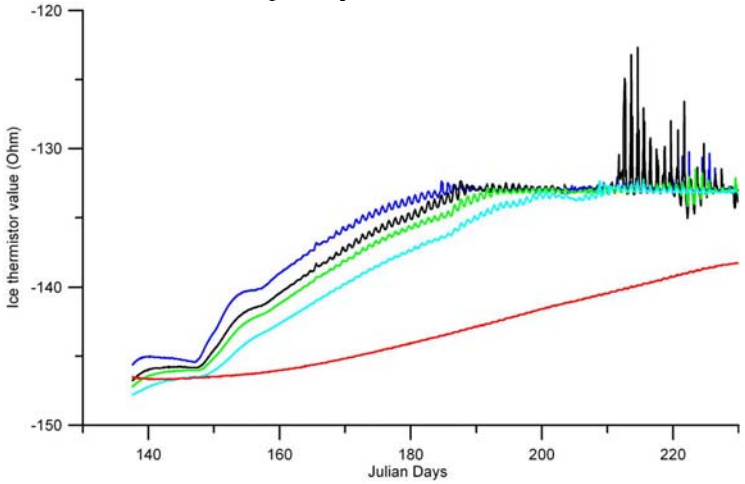

Figure 3.2.4: Thermistor data collected at the moulin site during the 2008 field season. Measurements were made at depths of 25 cm (blue), 50 cm (black), 75 cm (green), 1 m (cyan) and 4.5 m (red). Some of the thermistors were melted out. This is raw data that has not yet been analyzed.

3.2.3 One Dimensional Heat Advection-Conduction Model

A one dimensional advection – conduction model was programmed in order to analyze the impact of the annual snow cover. In Figure 3.2.5 a season long simulation can be viewed. AWS surface air temperature data from JAR1 is used as a surface boundary condition. The vertical advection term is set equal to the accumulation. The location of JAR1 is therefore assumed to be in steady state with a mass balance of zero. This is incorrect as JAR1 is in the ablation zone and will be changed in future studies but it is a useful assumption in order to test the model.

The simulation over estimates the temperature at the surface by approximately 1° Celsius at the beginning of the accumulation season in September and October. By the end of the season the model currently slightly underestimates the temperature. Currently this is the major problem that is being worked on as it is the fundament of a future model that shall be used to simulate the en-glacial temperature household and en-glacial water system in 2 or even 3 dimensions.

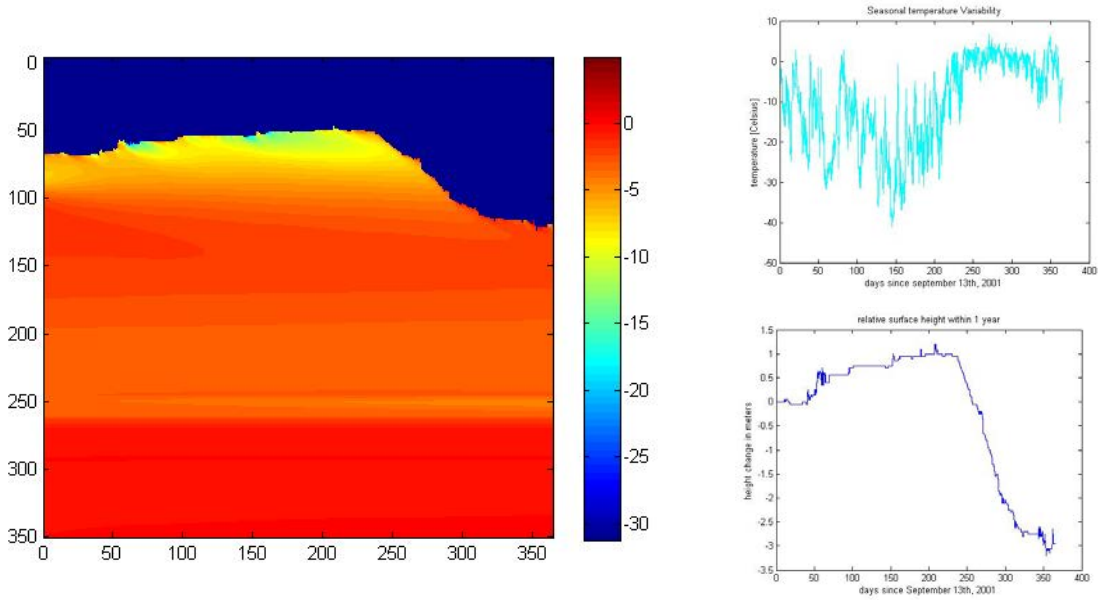

Figure 3.2.5: On the right is the temperature plot for the temperature of the ice sheet at JAR1. The upper right image shows the used surface air temperature forcing; the lower right image shows the surface height change for the same time period.

3.2.4 Spatial and Temporal Analysis of the Melt Area and Magnitude

In the final pilot project the magnitude of the different melt years and the mass balance for individual months where analyzed. The data for all years between 1996 through 2007 where used.

The plot starting in the upper left corner displays the mass balance for each month from July 1997 through July 2006. In the second image the total height loss for each year is recorded. 2007 is underestimated in this graph: The science tower fell over because it was melted out at the beginning of August. A third of the temporal melt season was missed out on. A strongly negative trend for the region is visible from the available data. The third image shows the average mass balance for each month for 1996 through 2007 for each month as well as the minimum and maximum mass balance. The mass balances for the accumulation months have a smaller variability than during the melt season. The variation for July is the largest. This indicates that the largest difference for annual mass balances at JAR1 is driven by melt. In forth figure the two years with the smallest mass loss (1997) is compared to the season with the highest mass loss (2005). 2005 had more precipitation for February and March but much higher mass loss in June, July and August. A longer melt season is not visible in this graph but a more intense melting during the classic summer months.

The following images are MODIS false color infrared images containing band 1 (red) as red, band 4 (Near Infrared) as green and band 26 (Mid Infrared) as blue. The extent of ice and wet snow can be seen as violet coloring. The spatial extent of melt for 2004 is larger than the melt region for 2007 in the August images despite the later year having a much larger total mass loss in the area. The AWS data from JAR 1 will help to calibrate the melt volume and mass loss for the region.

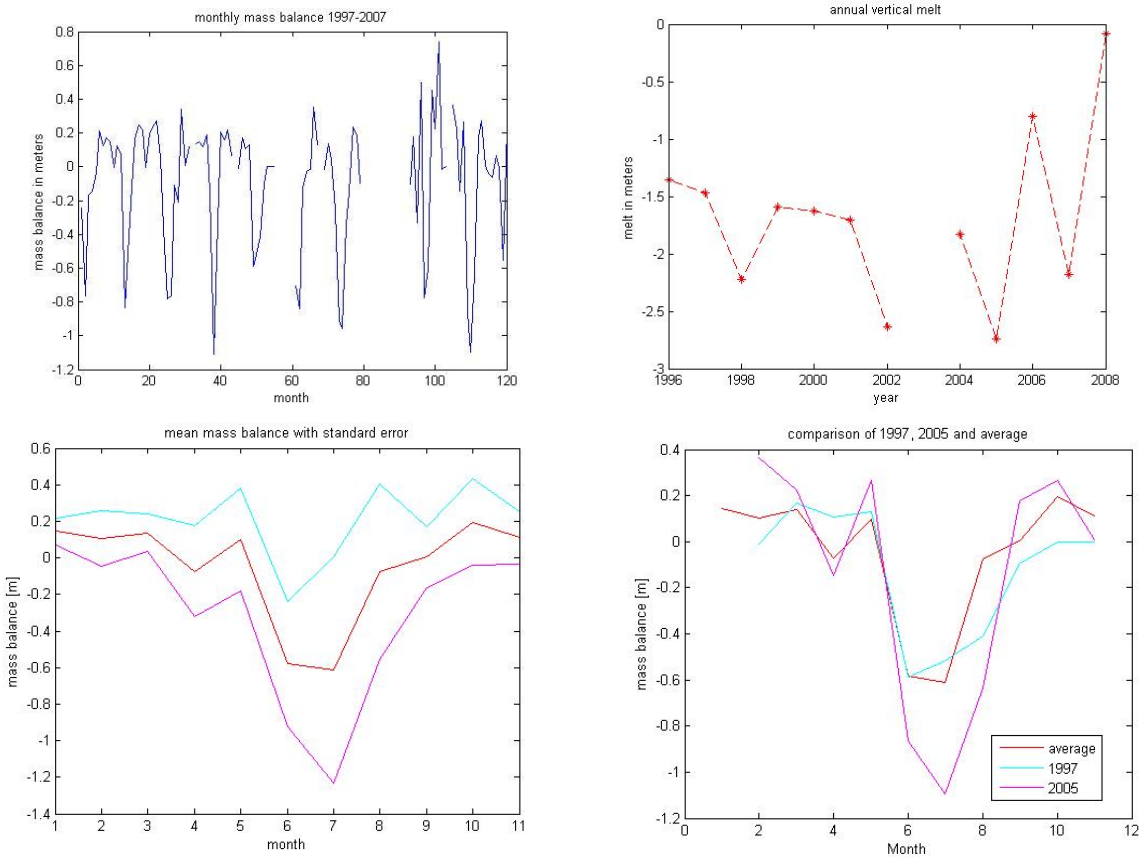

Figure 3.2.6: Clockwise, starting at the upper left image: monthly mass balance for June 1997 through July 2006. The short but intense melt season can be recognized for their sharp downward looking peaks. 2nd image: total annual mass balance at JAR1. Lower right: mean monthly mass balance (in red) is compared to the lowest loss of mass (1997) and the highest mass loss (2005) recorded. 2007 was the largest mass loss but the record has missing data and could not be analyzed. Lower left: minimum, maximum and average mass balance for each month.

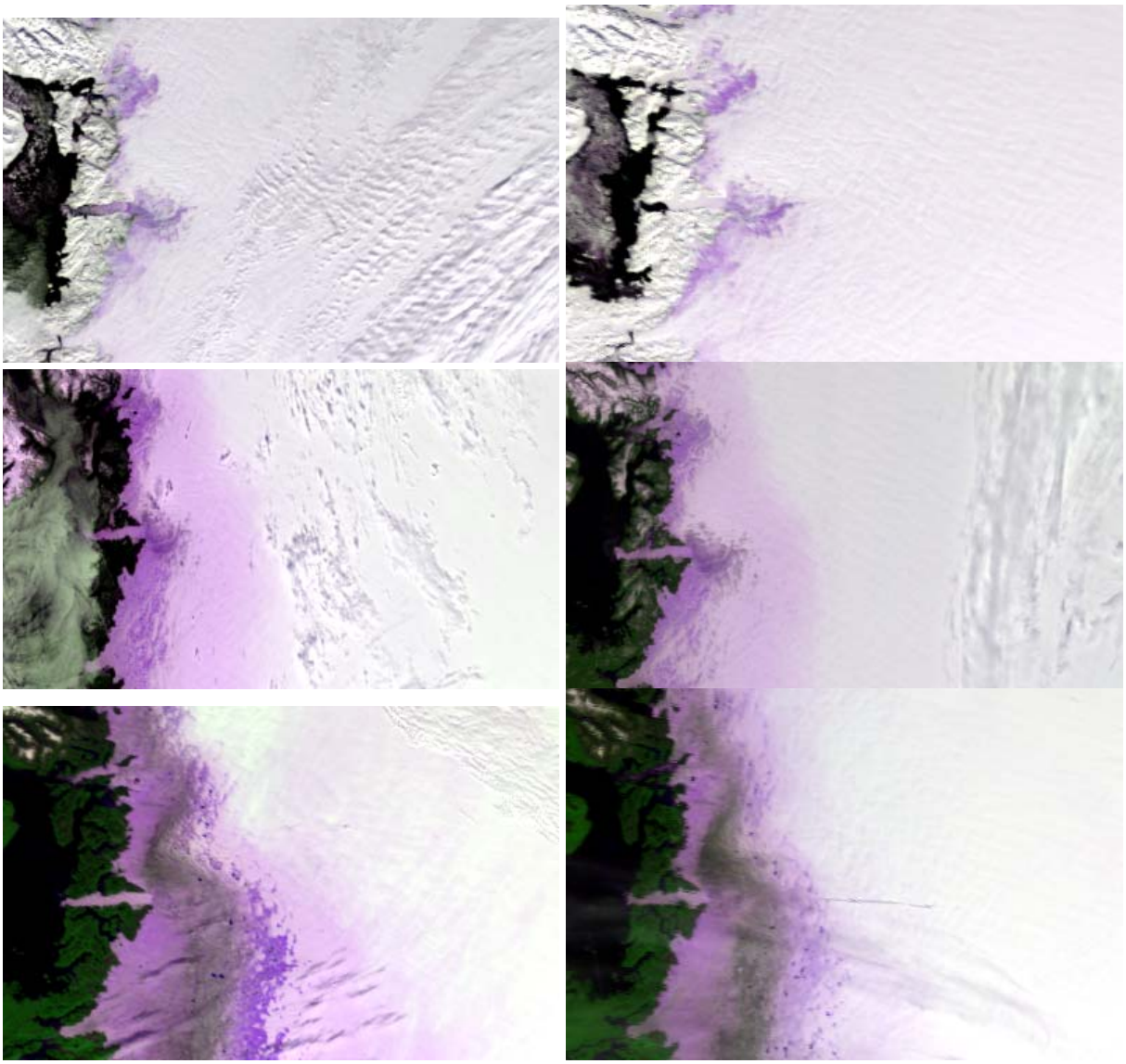

Figure 3.2.7: MODIS images using bands 1, 2 and 6 in order to high light the melt region with bare ice and wet snow facies. The images in the left column are 2004: April 10th, June 4th and August 13th. The right hand column contains the images for 2007 including April 9th, June 6th and August 10th.

3.2.5 Conclusion

The AWS dataset will be used as surface boundary condition and for the forcing of a model to simulate the the englacial water system. It will be used to get an estimate for available discharge, length of melt season and total water volume available to a moulin during a melt season. The surface boundary conditions will be based on this available data. In addition the data can be used to ground truth MODIS imagery in order to estimate the total melt area at a given time. The AWS data shows that the vertical change resulting in melt has a strong temporal gradient. The excellent temporal resolution of the AWS data set of hourly measurments allows us to analyze diurnal variations as well as diurnal cycles.

3.3 Sediment Plumes as a proxy for run-off from the Greenland Ice Sheet

In situ measurements to quantify run-off from the Greenland Ice Sheet (GrIS) are hindered by logistical difficulties associated with the large, remote and spatially diverse nature of the ice sheet. Modeling studies suggest that run-off accounts for approximately 50% of the annual mass loss from the ice sheet, however, there is a need to more accurately quantify run-off with empirical measurements. The purpose of this research was to determine if remote sensing could be used to characterize the onset, duration and intensity of run-off. The primary field site is Sondre Stromfjord, the longest fjord in Greenland, into which the Watson River flows, which drains approximately 6,300 km^2 of the ice sheet. The onset and duration of runoff into Sondre Stromfjord was compiled from Band 1 (620-670 nm, 250 m resolution) of the MODerate-resolution Imaging Spectroradiometer (MODIS) from 2001-2008. This study demonstrated that over this 8 yr period the onset of plume formation occurred earlier, with the onset occurring 9 days earlier in 2008 compared to 2001. The onset of the plume is intrinsically related to the onset of melt, supported by a positive correlation (r^2=0.82) between the formation of the plume and the onset of ablation at the S5 (490 m asl, 6 km from ice margin) Kangerlussuaq Transect automatic weather station (2003-2007). There is a similar positive correlation (r^2=0.90) between the cessation of ablation and the settling of the plume. Sediment plume area and concentrations in 2008 were mapped using a relationship between in situ suspended sediment concentrations (SSC) and reflectance values from MODIS.

3.3.1 Field Site

Research was conducted in the Sondre Stromfjord-Watson River-Russell Glacier system in west Greenland (67° N, 50° W). This region is characterized by ~150 km wide tundra, ~100 km wide ablation zone and an average equilibrium line altitude of ~1500 m a.s.l. (*van den Broeke*, 2008). Locally, an approximately 6,300 km^2 basin of the ice sheet drains into this system, in which there are three AWS stations, located at 6, 38, 88 km from the ice sheet margin at elevations of 490, 1020 and 1520 m a.s.l. (*van den Broeke*, 2008). In general, stations 5 and 6 are in the ablation zone, with net annual ablations of -3.6 and -1.5 m.w.e., respectively, while S9 is close to the equilibrium line (*van den Broeke*, 2008). Sondre Stromfjord is 160 km in length, between 2 and 8 km in width and runs approximately WSW. The fjord is approximately 4.5 km in width at its head, gradually widening to 6-8 km over the first 60 km length, before narrowing to 1.5-2 km over the next 100 km. The Watson River (also referred to as Sandflugtdalen) runs approximately 27 km from the ice margin and converges with the Orkendalen River, prior to flowing into Sondre Stromfjord. The Orkendalen River flows approximately 31 km from the ice margin before the convergence. The combined discharge of the rivers, measured at Kangerlussauq, is between 30-500 m^3/s (Mernild *et al.*, 2008).

3.3.2 In Situ and Remote Sensing Data

Two field campaigns were conducted during the 2008 melt season in Sondre Stromfjord, Greenland. The first, on June 4, 2008 collected surface water samples along a 30 km out and back transect (Figure 3.3.1). A second transect, later in the melt season, was conducted on August 13, 2008. These surface samples were processed for suspended sediment concentration (SSC) in Boulder, CO (*Roesler*, pers. comm.). In addition to the surface samples a WetLabs turbidity sensor (700 nm) was mounted alongside the front of the boat to collect a continuous transect, which was calibrated with te results of the in situ point samples. This continuous transect was used to overcome the scale mismatch between the point samples and the 250 m MODIS resolution.

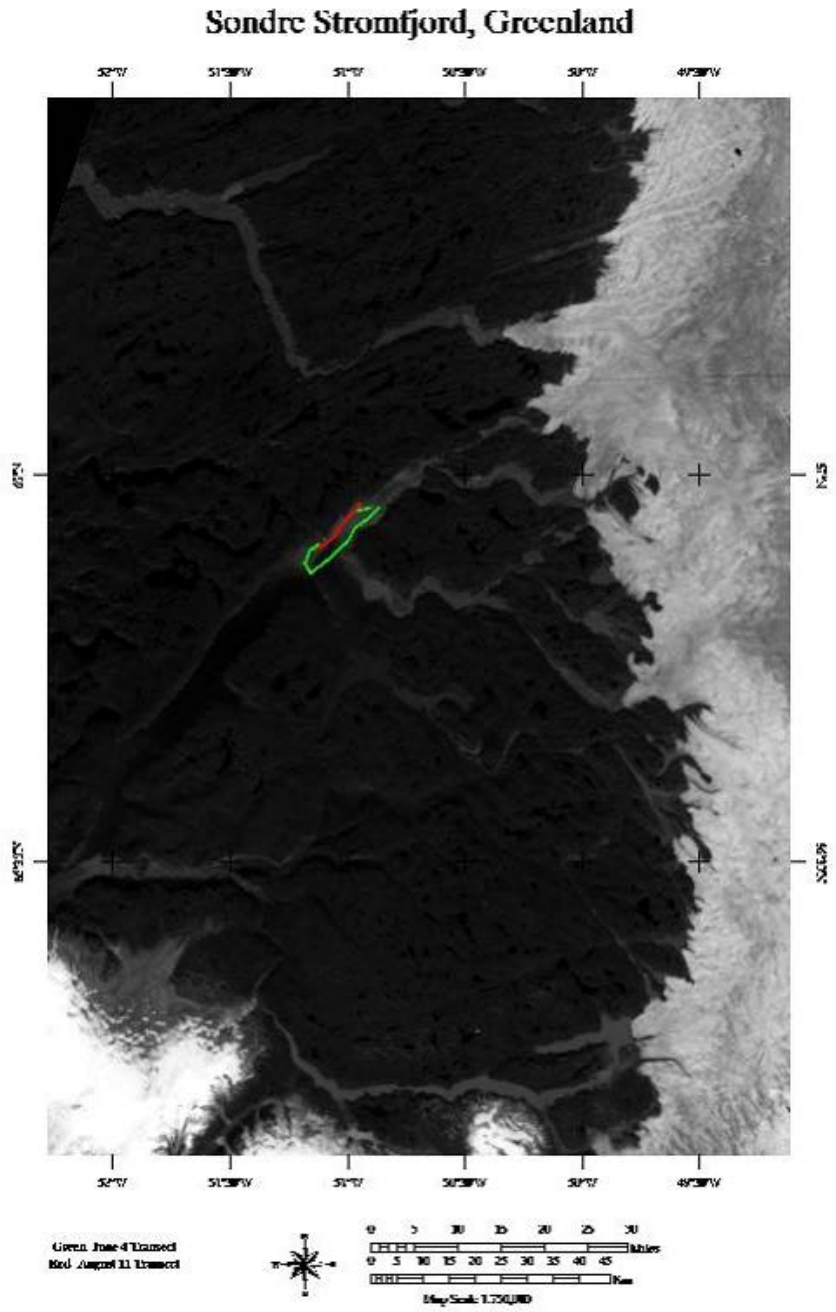

Figure 3.3.1:. Russell Glacier-Watson River-Sondre Stromfjord system, Greenland.

In situ measurements in the fjord were timed to correspond with a clear sky overpass of the MODIS instrument flying on the Terra platform on June 4th, 2008. Overcast conditions on August 13, 2008 resulted in a two-day offset between in situ sampling and a clear sky overpass of MODIS.

Clear sky Level 1B MODIS images were collected from 2001 to 2008, geo-referenced and processed using dark object subtraction for atmospheric correction. Band 1 offers the best combination of wavelength (620-670 nm) and resolution (250 m) for observing sediment plumes. Images were visually examined to determine the onset and cessation of the sediment plume in Sondre

Stromfjord. Error was introduced due to periods of extended cloud cover and/or a late break up of sea ice.

Data from the Kangerlussauq Transect Automatic Weather Stations provide in situ measurements of common meteorological parameters (*van den Broeke et al.*, 2008). These stations were installed in 2003 as a contribution to the GC-Net AWS network (*Steffen and Box*, 2001). Melt rates at Stations 5 (6 km from ice edge, 490 m asl) and 6 (38 km, 1020 m asl) were used to elucidate the connections between ablation and discharge (Figure 3.3.2).

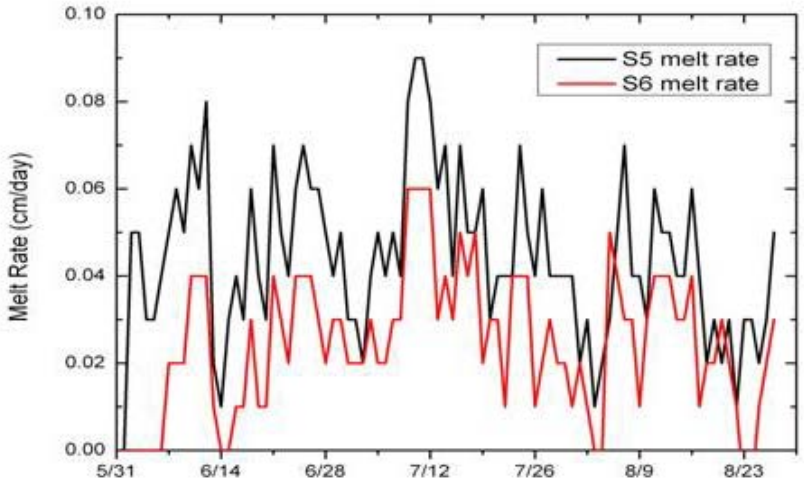

Figure 3.3 2. Melt Rate at K-Sec Stations S5 and S6 during 2007. Data courtesy of van den Broeke et al., 2008.

A third component of this integrated system is discharge from the Watson River into Sondre Stromfjord, which is collected at a gauging station located at a bedrock constriction in Kangerlussauq (*Mernild et al.*, 2008). Discharge increased from a background of ~30 m^3/s to peak at ~500 m^3/s in mid-July (Figure 3.3.3). The dramatic increase in discharge on August 31 is due to a jokalhaup at the edge of the Russell Glacier (*Mernild et al.*, 2008).

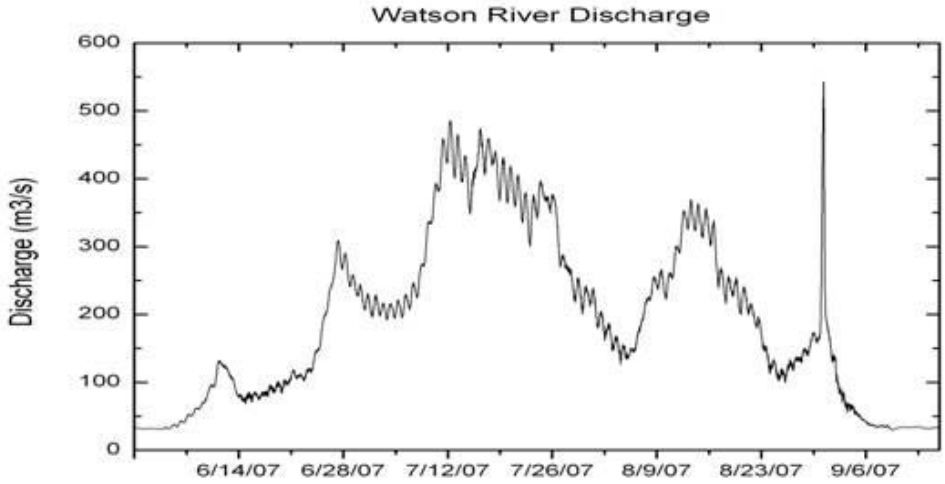

Figure 3.3. 3. Watson River discharge. Courtesy of Mernild and Hasholt, 2008.

3.3.3 Results and Discussion

The first step in developing the use of sediment plumes as a proxy for ice sheet runoff is investigating the relationship between ice ablation and discharge. The increased area undergoing surface melt as the summer progresses is responsible for the overall pattern of discharge but inherently masks the changes in ablation rate. However, by examining the derivative of the discharge it is easier to elucidate the connection to daily changes in the ablation rate (r^2=0.6, Figure 3.3.4).

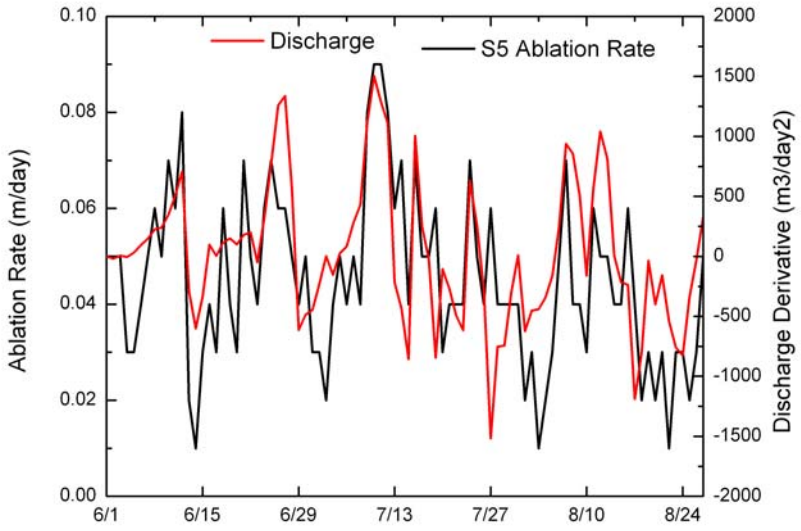

Figure 3.3.4. Comparison between ablation rate at K-Sect S5 and daily changes in Watson River discharge.

The consistent relation between ablation and discharge suggests that discharge is an adequate proxy for ablation when such in situ measurements are not available. However, there are very few locations in Greenland that measure river discharge, so it is necessary to go one step further to develop a proxy for discharge that can be measured remotely. Sediment plumes are tear shaped surface hydrologic features formed when sediment rich rivers drain into a receiving basin. The suspended sediment reduces optical depth and increases reflection making them distinct visual features commonly found along the coast of Greenland.

Point samples collected in Sondre Stromfjord were processed for SSC and correlated with reflectance values from geo-referenced, processed MODIS Band 1 data. There is a strong (r^2=0.89) exponential correlation between SSC and MODIS reflectance values (Figure 3.3.5). At higher SSC values, subsequent increases in SSC do not result in equivalent increases in MODIS reflectance value. This oversaturation is a limitation of using MODIS Band 1 to observe high concentrations of suspended sediment. A further step in the analysis is to incorporate the data transects collected with the WetLab's turbidity sensor.

The strong correlation between in situ SSC and MODIS reflectance values allows for the use of MODIS to observe plume formation and development. On average, plume onset occurred 9 days earlier in 2008 compared to 2001, similar to the findings of Hall et al. (2008). As discussed earlier, plume onset is intrinsically related to ablation onset on the ice sheet, which is supported by a strong correlation to ablation onset at the S5 AWS station (r^2=0.82) (Figure 3.3.6).

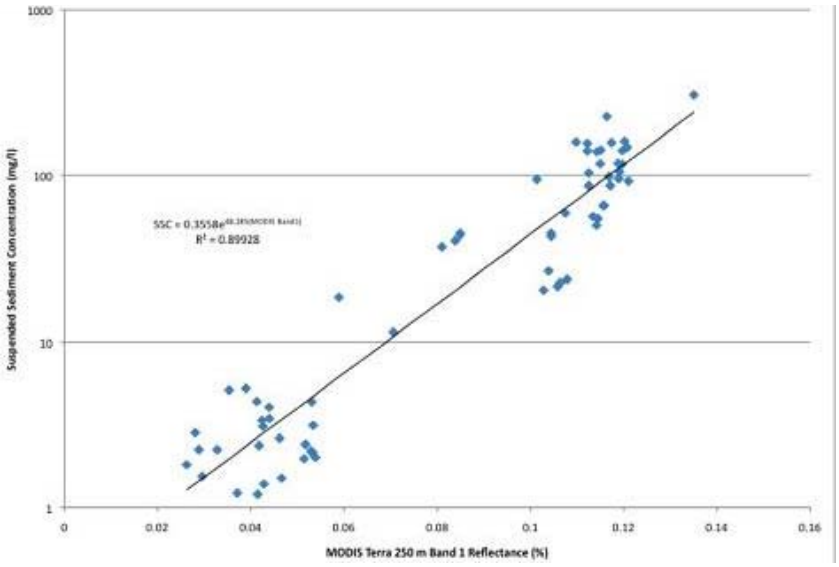

Figure 3.3 5. Correlation between MODIS Band 1 Reflectance and Suspended Sediment Concentration (mg/l). r^2*=0.89, n=66.*

Ongoing work focuses on reconstructing sediment plume characteristics (area and concentration) throughout the 2007 and 2008 melt seasons. These reconstructions are being compared to Watson River discharge data in order to further develop the relationship between the sediment plume and runoff from the ice sheet, manifested as Watson River discharge.

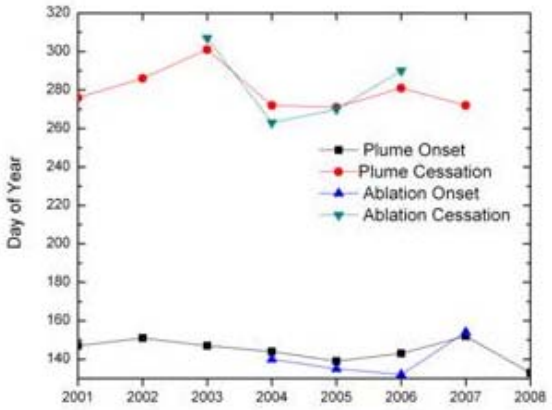

Figure 3.3 6. Onset and cessation of sediment plume in Sondre Stromfjord observed from MODIS Band 1. Onset and cessation of ablation at K-sect S5 is also plotted.

4. The Geodetic Measuring Program 2008

4.1 Introduction

The glaciological geodetic program to determine flow velocity, deformation and elevation change of the inland ice in the western part of the Greenland ice sheet was carried out by 3 members of Stuttgart University of Applied Sciences between August 1st and August 15th, 2008. State and results of previous campaigns until 2006 were reported in *Stober and Hepperle*, 2007.

There are two main research areas: The first research field at Swiss Camp (ETH/CU-Camp) was started in 1991. Until 2008 a total of 10 campaigns were carried with repeated measurements of a stake network. It consists of 4 stakes (triangle with 1 point in its centre). The second research field was established in 2004. It has the same net design as at Swiss Camp (4 stakes, triangle with 1 point in its centre). ST2 is situated in latitude = 69° 30' 28" N; longitude = 49° 39' 09" W, ellipsoidal height = 1000 m, hence 170 m lower than Swiss-Camp, approximately 14 km south-west from Swiss-Camp and approximately 1,5 km up-glacier from JAR1. Here we have now four campaigns in 2004, 2005, 2006, and 2008.

The measuring program 2008 was similar to previous campaigns. All GPS measurements were done by 2 receivers Leica System 500 and 2 receivers Leica System 1200, with real-time equipment. The program 2008 consisted in:

4.1.1 Local GPS measurements in Ilulissat

- GPS reference point EUREF-0112 in Ilulissat on solid rock,
- Long-time GPS measurement in order to investigate GPS multipath effects and ionospheric interferences of GPS-signals.
- Local GPS network in order to study GPS accuracy in high latitudes.
- Determination of point EUREF-0112 in the International Terrestrial Reference Frame (ITRF).

4.1.2 ST-2 (August 8th, 2008)

- Static GPS baseline 65 km to EUREF 0112 in Ilulissat, measured for 8 hours,
- Temporal ice GPS reference near central stake ST200,
- All 4 stakes had been melted out. New aluminium stakes were installed at supposed old positions by 4 meter deep drilling,
- Measurement of the actual positions of all 4 stakes ST200 (new ST280), ST201 ((new ST281), ST202 (new ST283), and ST203(new ST283) ,
- Reconstruction and staking out of old positions from 2004, 2005, and 2006.
- Measuring actual heights at all these old positions by real-time GPS
- Topographical survey of ice surface (no snow cover left) by grid points every 200 meters and kinematic GPS profiling, area 1.6 x 1.6 km^2.

4.1.3 Swiss Camp (August 11th, 2008)

- Static GPS baseline 80 km to EUREF 0112 in Ilulissat, measured for 7 hours,
- Temporal ice GPS reference (point 106.1) at Swiss Camp for real-time GPS around Camp area,

- All 4 stakes had been melted out. New aluminium stakes were installed at supposed old positions by 4 meter deep drilling,
- Measurement of the actual position of replaced points.
- Reconstruction and staking out of old positions from 1994, 95, 96, 99, 2002, 2004, 2005, and 2006.
- Measuring actual heights at all these old positions by real-time GPS,
- Measuring of snow depth in order to reduce heights to ice surface,
- Topographical survey of ice surface (no snow cover left!) around Swiss-Camp by grid points every 200 meters and kinematic GPS profiling.

4.1.4 Flow velocity of the outlet glacier "Eqip Sermia" (August 6th and 13th , 2008)

- Photogrammetry on two camera stations, baseline 120 m,
- absolute and relative GPS-positioning of camera stations,
- repetition of measuring procedure after 7 days .

4.2 Results

4.2.1 Swiss Camp Area

The measurements in 2008 had been carried out on August 11th, with an air temperature of + 2°C. The surface was dry, but with a lot of superficial water in small rivers. It was first year when all snow was melted, and there was no remaining snow layer. All measurements were done directly on the ice horizon. All heights are absolute heights (reference point EUREF 0112 in Ilulissat on solid rock).

Elevation changes were derived from concrete previous point positions. Figure 4.1 shows the elevation change from concrete (previous) stake point positions**.**

The adjusted straight line (Figure 4.1, dashed line) over the whole period 1991 - 2008 shows an average elevation change of –0.36 m/a. Temporal variations up to a decrease of –0.85 m/a according to higher summer air temperature are clearly visible. All the extremely big elevation changes 1995-1996 and 2002-2004 coincide with the highest summer air temperatures. Between the last campaigns 2006-2008 we find an extreme elevation decrease of –1.04 m per year, which is three times greater than the average from all years. In the period 1991 until 2002 the linear trend was –0.22 m/a. The smoothed polynomial curve (fig. 4.1, red) shows an accelerated elevation decrease, especially in the last warm years. Since the beginning of our research in 1991 the ice horizon has been lowered by a total of –6.66 m.

The topographical survey 2008 **(**Figure 4.2) was carried out North-West from the Camp. The measured area is situated closer to the camp than in former years in order to reduce long walks. Hence, this year we get an digital elevation model which is not coinciding with the previously measured area, and elevation changes from the difference digital elevation models 2006-2008 are not available, but we have a good basis for future comparisons.

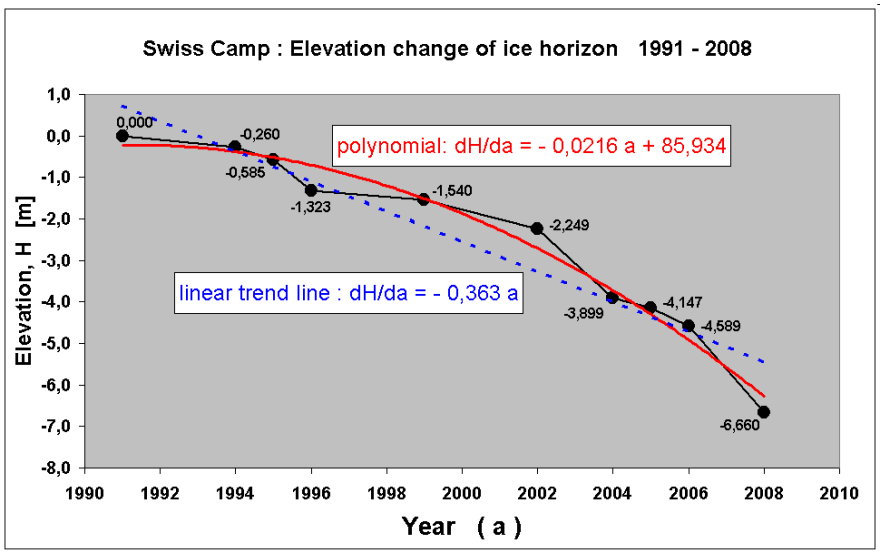

Figure 4.1: Swiss Camp: Elevation change of ice horizon 1991 – 2008

The terrain in the 2008 measured part is smooth with an average declination of 1.8%.

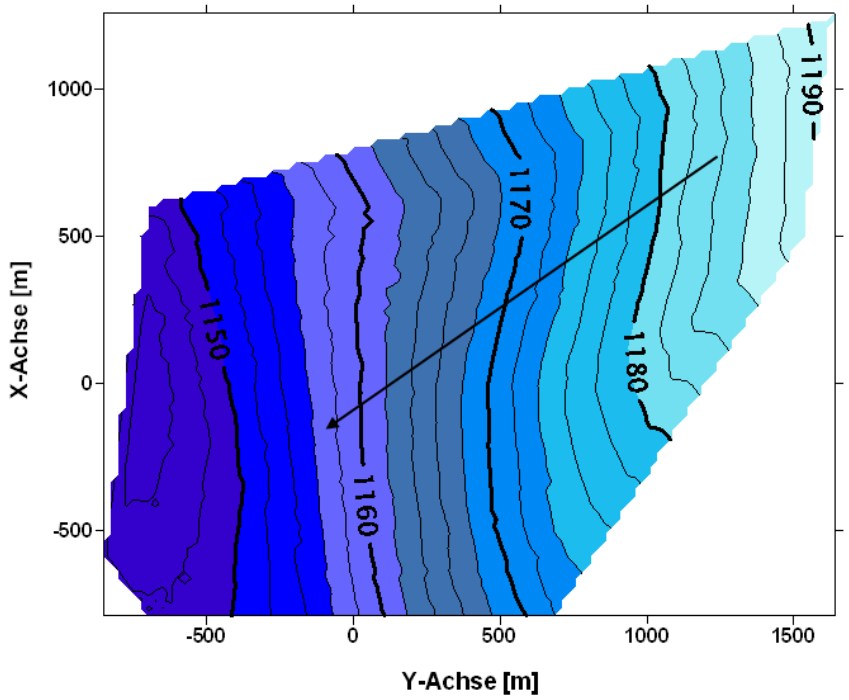

Figure 4.2: Contour map at Swiss-Camp, topographical survey 2008. Local coordinate system with origin at Swiss-Camp 1999; arrow = ice flow direction.

The ice flow vector is determined by comparison of stake positions in different years. Between 2006 and 2008 it can not be determined exactly, because in 2008 all stakes were melted out due to extreme ablation rates. The new stakes were installed at the old positions as good as possible. The new stake network is a precise basis for the next campaign. With these restrictions the flow velocity between 2006 and 2008 has a limited accuracy.

The resulting ice flow velocity in average is 0,317 m/d. With one exception, 1995-1996, we find continuously increasing values with years (Figure 4.3), probably due to more melt water at the bottom with increased sliding on the bedrock (*Zwally et al.*, 2002).

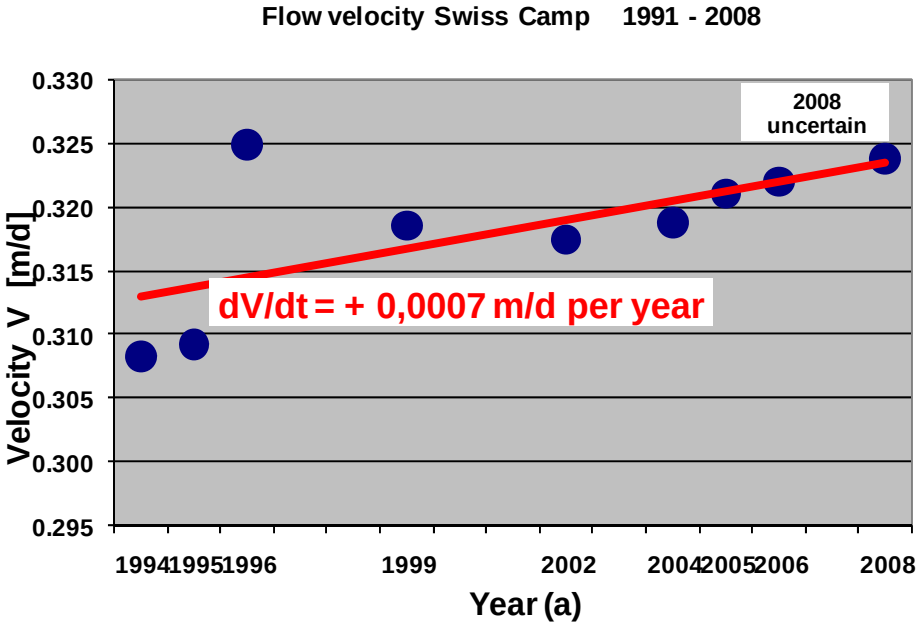

Figure 4.3: Swiss Camp: Ice flow velocity [m/d], 1991 – 2008

In summary, our results indicate an accelerated elevation lowering and melting (ice thickness lowering), especially in the last years, with some extremely high rates during warm summers. This is in agreeing with the observed global warming, and in particular increasing temperatures in Polar Regions.

4.2.2 ST2 Area

The area "ST2" is situated in 1000 m altitude, 150 m lower than "Swiss Camp". This research field was established in 2004 and re-measured in 2005, 2006, and now 2008. At the time of the measurement (August 8th, 2008) the surface was hard and without melt water; there was no snow cover left over the ice surface. All measurements were directly referred to the ice horizon. All stakes were melted out, due to extremely high ablation rates. New stakes (4 meter deep) were planted again at the correct positions

The elevation change was derived from digital elevation models (area 1.6 x 1.6 km^2) in all campaigns, using grid points every 200 meters, and some kinematics GPS profiles. In average, between 2004 and 2005, we had got an elevation decrease –0.38 m/a, and between 2005 and 2006 –0.30 m/a. Now, between 2006 and 2008, we got an elevation decrease of –1.40 m/a. Figure 4.4 shows the temporal variation 2004 – 2008 at ST2. It clearly indicates the accelerated lowering of the ice surface in the last years.

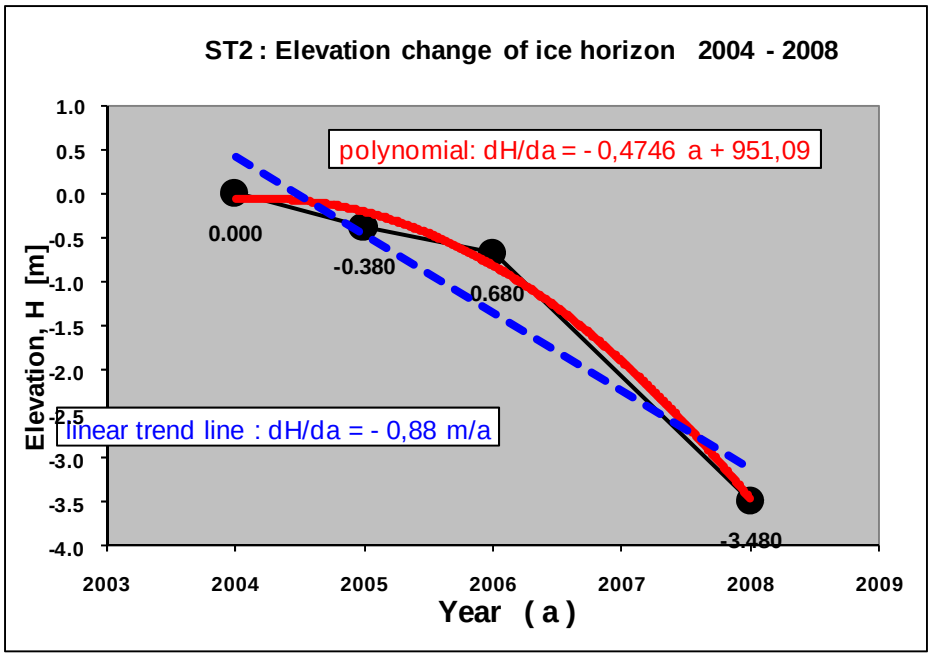

Figure 4.4: Area ST 2 : Elevation change of ice horizon 2004 – 2008

The elevation change varies locally over the whole area. As an example, in Figure 4.5 the differential digital elevation model 2006-2008 is shown. In some parts we see an elevation change from – 1.8 to – 4 m, and in average –2.8 m. The ice flow velocity of area "ST2" in average from all 4 stakes is shown in Figure 4.6. In average the flow velocity is 0,197 m/d with a flow azimuth 266.4 gon. In contrast to Swiss Camp, at ST2 the flow velocity is much slower, and not increasing with years. The slower ice movement is typical for areas below the equilibrium line where we can expect a maximum.

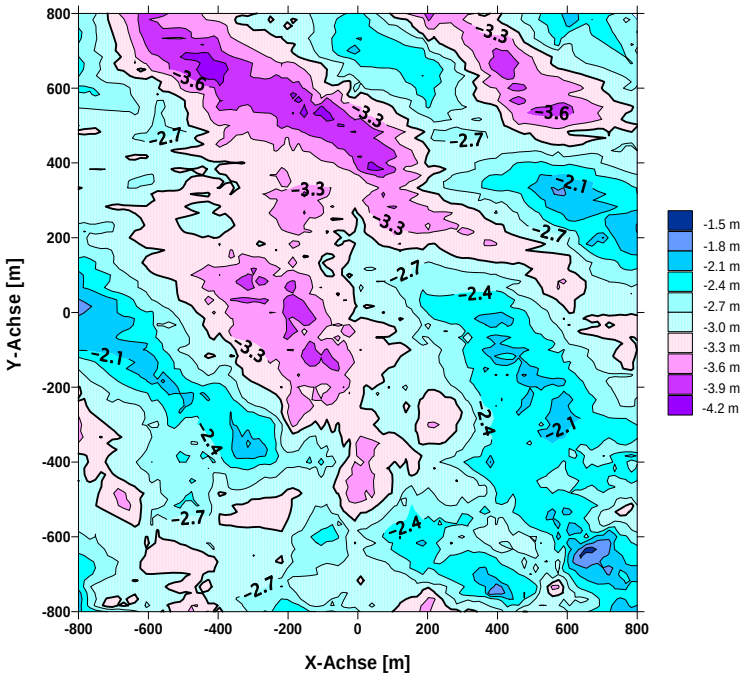

Figure 4.5: Differential elevation model at ST2, topographical survey 2008. Local coordinate system (origin ST200 in 2004).

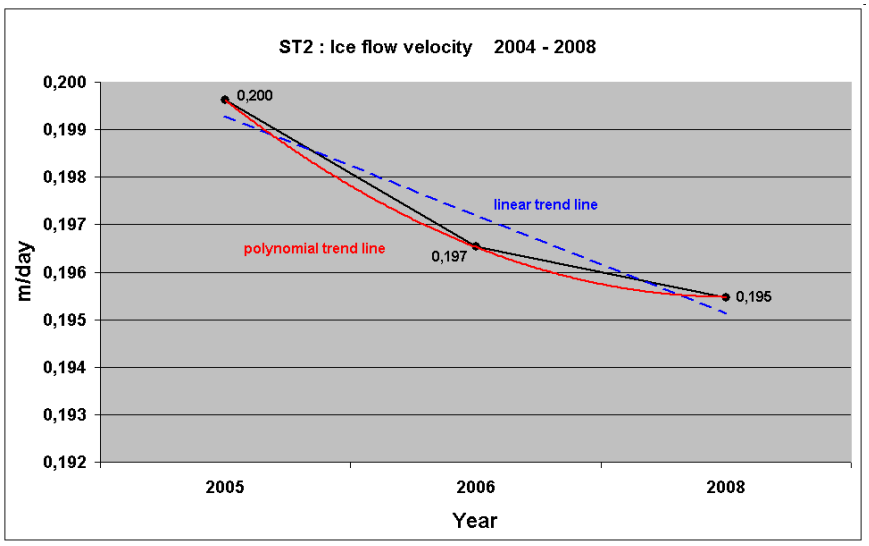

Figure 6: Area ST2: Ice flow velocity [m/d], 2004 - 2005 - 2006 - 2008

In summary, the results of both research areas (Table 4.1) from the periods since the beginning of our observations (Swiss Camp: 1991, ST2 : 2004) show about the same trend in elevation decrease - 0,32 m/a, respectively – 0.34 m/a. But between the last campaigns (2006-2008) in both areas we find an extremely big lowering of the ice surface with -1.04 m/a, respectively –1.40 m/a. The recent ice thickness loss is more than three times greater than the long-term trend in former years. The mass budget is negative. It demonstrates the high sensitivity of increasing air temperature, especially in the ablation area near the ice margin.

The flow velocities and therefore ice mass transport are different. At Swiss-Camp we recently get slightly increased now 0.32 m/d (uncertain due to reconstructed stake positions), and unchanged 0.20 m/d at ST2.

	Swiss-Camp (ell. alt.= 1170 m)		ST2 (ell. altitude = 1000 m)	
	2006 - 2008	Trend 1991-2006	2006 - 2008	Trend 2004-2006
Elevation change [m/a]	-1,04	-0,32	-1,40	-0,34
Flow velocity [m/d]	0,324 (?)	0,318	0,195	0,198

Table 4.1 : Comparison of Swiss-Camp and ST2, elevation change and flow vectors

4.3 Evaluation and Validation of ICESat data

Both research areas, ST2 and Swiss camp as well, are precisely measured parts of the Greenland ice sheet. Therefore they can be also used for evaluation and validation of satellite elevation data, especially for ICESat. For this purpose our height results have to be transformed in the worldwide used International Terrestrial Reference Frame (ITRF) which is also used for the satellite results. Our reference point EUREF0112 in Ilulissat was originally coordinated in the EUREF-campaign in 1990. Due to the early state of GPS evolution the resulting accuracy was very limited at those times. A new coordination with three points of the International Geodynamic Service (IGS) gives a

height correction of –1.16 m for point EUREF0112, and therefore also for all our measurements on the ice sheet.

In 2008 no identical flight tracks of ICESat over Swiss Camp or ST2 were available. In 2005, on May 21, the ICESat flew over a part of the Swiss Camp topographically measured area (Figure 4.7). In the north-western part we can compare heights measured by the satellite ICESat (GLAS Laser L3C), and by terrestrial control survey as well **(**Table 4.2**)**. In average from 5 points, the GPS heights are 2.81 m lower than the ICESat heights. Due to lack of snow cover data, in these preliminary results no correction due to seasonal changes of snow layer thickness is not taken into account. Unfortunately a real validation for the same snow conditions is not possible. From snow pits in earlier campaigns we can assess a possible snow layer in May of about 2 meters over the ice horizon. The terrestrial GPS measurements in August are referred on the ice horizon. Hence, a systematic bias of approximately 0.8 meters would remain in the ICESat heights.

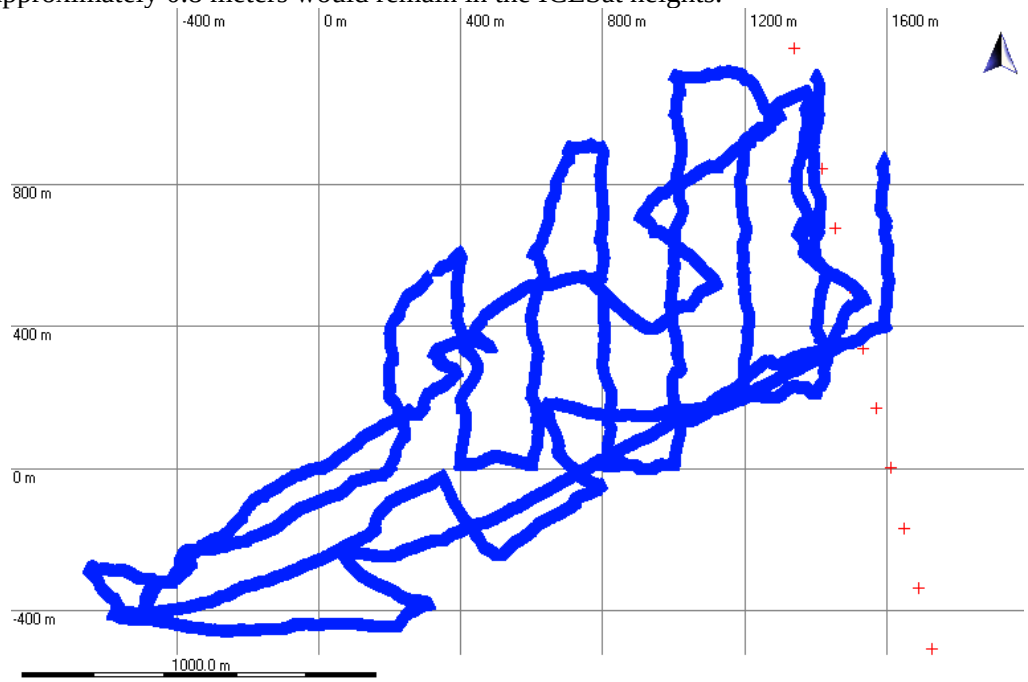

Figure 4.7: Kinematics topographical GPS survey at Swiss Camp 2005 (blue tracks) and footprints of ICESat 2005 (red crosses).

ICESat, Point No.	Kinematic GPS on ice horizon, point No.	Horizontal distance between points [m]	Height difference, ICESat - GPS, ITRF = ΔH [m]
May 21, 2005	**August 4, 2005**		
2255	13771	30,9	2,65
2256	27761	13,6	2,35
2257	12097	47,5	3,32
2258	12376	24,1	2,78
2259	26648	5,2	2,81
2260	12716	95,0	1,87
Ave. 2255-2259		**24,3**	**2,78**

Table 4.2: Height difference and horizontal distance between ICESat and kinematics GPS points at Swiss Camp in 2005.

4.4. Flow Velocity of Eqip Sermia Glacier

The flow azimuth of Swiss-Camp and ST2 shows an ice flow towards the glacier Sermeq Avangnardleg ("North Glacier"), which is belonging to the catchment basin of Jakobshavn Isbrae glacier (Figure 4.8). This glacier is actually thinning and has doubled its speed since last 10 years (*Joughin et al.* 2004, *Maas et al.* 2006). In order to compare flow velocities of different outlet glaciers, we decided in 2005 and again 2008 to determine the recent flow velocity of the Eqip Sermia, situated only 80 km north from the Jakobshavn Glacier. The geographical location is shown in Figure 4.8. The repeated terrestrial photogrammetric observations had been carried out on August 6th and 13th at two camera positions on the moraine along the southeast glacier margin.

As measuring technique the terrestrial photogrammetry was applied with following features:

- Baseline for stereophotos = 120 m, on side moraine near glacier front,
- Digital camera Canon EOS 350D, camera calibration by PhotoModeler,
- absolute and relative GPS-positioning of camera stations,
- repetition of measuring procedure after 7 days
- Evaluation by software Summit Evolution.

Point No.	Distance	displacement per day
1	2300 m	3,64 m
2	770 m	4,15 m
3	600 m	3,94 m
Average		**3,91 m**

Table 4.3: Flow velocities from Eqip Sermia Glacier , August 2008.

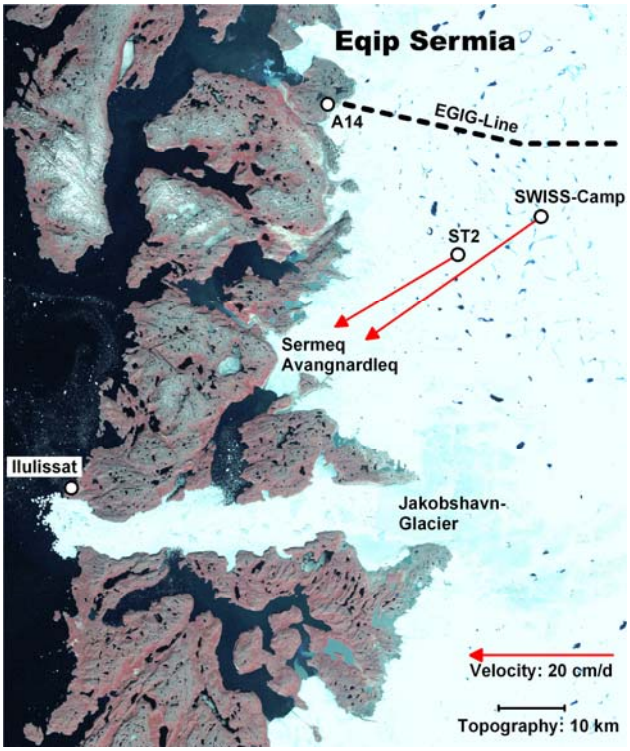

Figure 4.8: Research areas and ice flow vectors (Landsat image, July 7th , 2001)

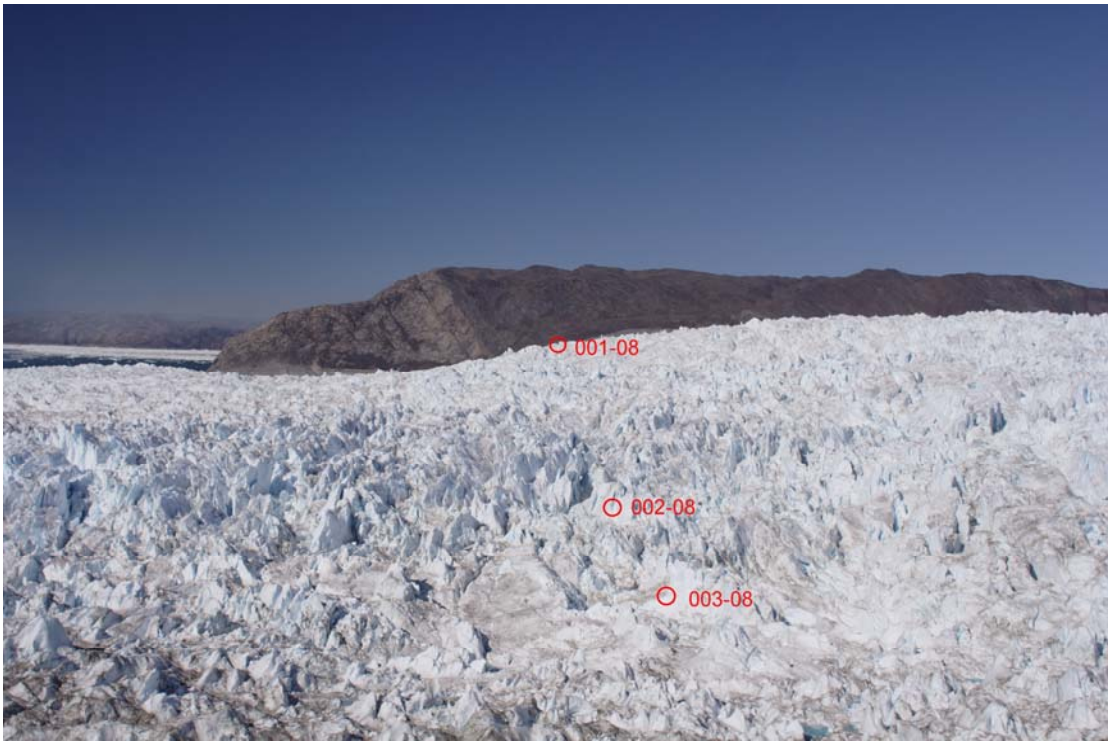

Figure 4.9: Terrestrial photogrammetry at the Eqip Sermia outlet glacier, view from south east moraine, August 6th 2008.

The view (Figure 4.9) shows the sight line across the lower part of the glacier together with 3 selected measured points. The wideness of the whole glacier is here about 4 km, hence our visible points reach the glacier surface until the central flow line.

In average (Table 4.3) the glacier flows with a speed of 3,9 m per day in summer 2008. Compared to 3.5 m/d in 1959 (BAUER 1968) there is only little change in velocity. In the same part of the glacier, ZICK 1972 reported the average flow velocity 3.6 m/d in July/August 1971. Compared to other authors and other methods, we can not confirm the results from satellite radar interferometry observations, e.g. by *Rignot et al*. 2006, who reported an acceleration from 1.9 m/d in October 2000 up to 2.5 m/d in April 2005.

Contrarily to the huge recent velocity acceleration of the Jakobshavn Isbrae glacier we can also not confirm similar glacier flow acceleration for the Eqip Sermia. Summarizing the Eqip Sermia shows a very stable behaviour, while Jakobshavn Isbrae changes speed, thickness and front completely. In spite of similar climate change in the whole area, glaciers obviously react in a very different way on climate change.

5. Bibliography

Abdalati, W., and K. Steffen, Passive microwave derived snowmelt regions on the Greenland ice sheet. *Geophysical Research Letters* 22(7), 787-790, 2001.

Arnold, N. and M. Sharp, Flow variability in the Scandinavian Ice Sheet: modeling the coupling between ice sheet flow and hydrology. *Quat. Sci. Rev.* 21: 485-502, 2001.

Bauer, A.: Le glacier de Eqe (Eqip Sermia) mouvement et variations du front (1959). Meddelelser om Groenland, Vol. 174, Nr. 2, Koebenhavn 1968.

Bamber, J., S. Ekholm and W. Krabill, A new, high-resolution digital elevation model of Greenland fully validated with airborne laser altimeter data. *J. Geophys. Res.* 106: 6733-6745, 2001.

Box, J.E. and K. Steffen, Sublimation on the Greenland ice sheet from automated weather station observations. *J. Geophys. Res.*, 106(D24), doi:10.1029/2001JD900161, 2001.

Flowers, G., and G. Clarke, A multi-component coupled model of glacier hydrology. *J. Geophys. Res.* 107(B11), doi:10.1029/2001JB001122, 2002.

Hall, D., S. Williams, S. Luthcke, and N. Digirolamo. 2008. Greenland ice sheet surface temperature, melt and mass loss: 2000-2006. *Journal of Glaciology*, Vol. 54, No. 184, 81-93.

Hanna, E., P. Huybrechts, K. Steffen, J. Cappelen, R. Huff, Ch. Shuman, T. Irvine-Fynn, S. Wise, and M. Griffiths, Increased runoff from melt from the Greenland Ice Sheet: a response to global warming. *J. Climate.* 21: 331-341, 2008.

Joughin, I., W. Abdalati, M. Fahnestock: Large fluctuations in speed on Greenland's Jakobshavn Isbrae glacier. *Nature*, 432, 608-610, 2004.

Maas, H.-G., R. Dietrich, E. Schwalbe, M. Bäßler, P. Westfeld: Analysis of the motion behaviour of the Jakobshavn Isbrae glacier in Greenland by monocular image sequence analysis IAPRS Vol. XXXVI, Part 5, 179-183, Dresden , September 2006.

Marshall, S., Recent advances in understanding ice sheet dynamics. *Earth Plan. Sci. Lett.* 240: 191-204, 2005.

Marshall, S., H. Björnsson, G. Flowers and G. Clarke, Simulation of Vatnajökull Ice Cap dynamics. *J. Geophys. Res.* 110(F03009), doi:10.1029/2004JF000262, 2005.

Mernild, S. H., Hasholt, B., Kane, D. L., and Tidwell, A. C. 2008. Jökulhlaup Observed at Greenland Ice Sheet. *Eos Trans*. AGU, No.99, 321–322.

Nghiem, S.V., K. Steffen, R. Kwok, and W.Y. Tsai, Diurnal variations of melt regions on the Greenland ice sheet, J. Glaciol., 47(159), 539-547, 2001.

Plummer, J., S. Gogineni, C. van der Veen, C. Leuschen and J. Li, Ice Thickness and bed map 462 for Jakobshavn Isbrae, CReSIS Tech Report #2008-1, 2008.

Price, S., A. Payne, G. Catania and T. Neumann, Seasonal acceleration of inland ice via 464 longitudinal coupling to marginal ice. *J. Glaciol*. 54: 213-219, 2008.

Rignot, E. and P. Kanagaratnam, Changes in the Velocity Structure of the Greenland Ice Sheet. *Science.* 311: 986-990, 2006.

Roesler, C. 2007. Personal Communication.

Scambos, T. and T. Haran, An image-enhanced DEM of the Greenland ice sheet. 2002. *Ann. Glaciol.* 34: 291-298, 2002.

Shuman, C., K. Steffen, J. Box, and C. Stearn, A dozen years of temperature observations at the Summit: Central Greenland automatic weather stations 1987-1999, *J. Appl. Meteorol*., *40*(4),741-752, 2001.

Steffen, K. and J. Box, Surface climatology of the Greenland ice sheet: Greenland Climate Network 1995-1999, *Journal of Geophysical Research* 106(D24), 33,951-33,964, 2001.

Stober, M. , and Hepperle, J.: Changes in Ice Elevation and Ice Flow-Velocity in the Swiss Camp Area (West Greenland) between 1991 and 2006. Polarforschung 76 (3), p. 109 – 118, 2006, erschienen 2007.

Thomsen, H., L. Thorning and R. Braithwaite, Glacier-hydrological conditions on the Inland Ice north-east of Jakobshavn/Ilulissat, West Greenland. Grønlands Geologiske Undersøgelse. Rapport 138, 1988.

Tulaczyk, S., W. Kamb and H. Engelhardt, Basal mechanics of Ice Stream B, West Antarctica 1. Till mechanics. *J. Geophys. Res.* 105: 463-482, doi:10.1029/1999JB900329, 2000.

Van den Broeke, M. R., C. J. P. P. Smeets, J. Ettema and P. Kuipers-Munneke. 2008. Surface radiation balance in the ablation zone of the west Greenland ice sheet, *Journal of Geophysical Research*, Vol. 113, D13105, doi:10.1029/2007JD009283.

van der Veen, C, Longitudinal stresses and basal sliding: A comparative study. *Dynamics of the West Antarctic Ice Sheet*. ed. C. van der Veen and J. Oerlemans. p. 223-248, 1987.

Zick, W. : Eisbewegungen am Eqip Sermia und im westlichen Randgebiet des grönländischen Inlandeises (EGIG Arbeitsgebiet). Polarforschung, 42, 1, 24-30, 1972.

Zwally, H., W. Abdalati, T. Herring, K. Larson, J. Saba and K. Steffen, Surface melt-induced acceleration of Greenland Ice Sheet flow. *Science.* 297: 218-222, 2002.